Structural, Computational, and ^{59}Co NMR Studies of Primary and Secondary Amine Complexes of Co(III) Porphyrins

Orde Q. Munro,* Sibongiseni C. Shabalala, and Nicola J. Brown

School of Chemical and Physical Sciences, University of Natal, Pietermaritzburg, Private Bag X01, Scottsville, 3209, South Africa

Received August 28, 2000

Four novel low-spin bis(amine) Co(III) porphyrins [Co(TPP)($BzNH_2$)$_2$](SbF_6), **1**, [Co(TPP)(1-$BuNH_2$)$_2$](SbF_6), **2**, [Co(TPP)($PhCH_2CH_2NH_2$)$_2$](SbF_6), **3**, and [Co(TPP)(1-MePipz)$_2$](SbF_6), **4**, have been synthesized and characterized by low-temperature X-ray crystallography, IR, electronic, and NMR (^{1}H, ^{13}C, and ^{59}Co) spectroscopy. The mean Co−N_p distance for the four structures is 1.986(1) Å. The Co−N_{ax} distances for the 1° amine derivatives average to 1.980(5) Å; the axial bonds of the 2° amine derivative are significantly longer, averaging 2.040(1) Å. The porphyrin core conformation of **4** is significantly nonplanar (mixture of S_4-ruf and D_{2d}-sad distortions) due to a staggered arrangement of the axial ligands over the porphyrin core and *meso*-phenyl group orientations < 90°. The X-ray structures have been used with the coordinates for [Co(TPP)(Pip)$_2$](NO_3) (Scheidt et al. *J. Am. Chem. Soc.* **1973**, *95*, 8289−8294.) to parametrize a molecular mechanics (MM) force field for bis(amine) complexes of Co(III) porphyrins. The calculations show that two types of crystal packing interactions (van der Waals and hydrogen bonding) largely control the crystallographically observed conformations. Gas phase conformational energy surfaces have been computed for these complexes by dihedral angle driving methods and augmented with population distributions calculated by MD simulations at 298 K; the calculations demonstrate that the bis(1° amine) complexes are significantly more flexible than the bis(2° amine) analogues. ^{59}Co NMR spectra have been acquired for a range of [Co(TPP)(amine)$_2$]Cl derivatives as a function of temperature. The ^{59}Co chemical shifts increase linearly with increasing temperature due to population of thermally excited vibrational levels of the $^1A_1$ ground state. Activation energies for molecular reorientation (tumbling) have been determined from an analysis of the ^{59}Co NMR line widths as a function of 1/*T*; lower barriers exist for the conformationally rigid 2° amine derivatives (2.6−3.8 kJ mol^{-1}). The ^{59}Co chemical shifts vary linearly with the DFT-calculated radial expectation values $\langle r^{-3}\rangle_{3d}$ for the Co(III) ion. The correlation leads to the following order for the σ-donor strengths of the axial ligands: $BzNH_2 \geq Cl^- >$ 1-$BuNH_2 >$ $PhCH_2CH_2NH_2 >$ 1-$Bu_2NH >$ Et_2NH. The ^{59}Co NMR line widths are proportional to the square of the DFT-calculated valence electric field gradient at the Co nucleus. Importantly, this is the first computational rationalization of the ^{59}Co NMR spectra of Co(III) porphyrins.

Introduction

Although Co(III) porphyrins are not naturally occurring, they have become increasingly important as useful receptors for amines, amino acids, and other ligands.[1−3] Advantageous physical properties such as slow axial ligand exchange on the ^{1}H NMR time scale, a large diamagnetic ring current effect,[4,5] and negligible line broadening have resulted in the use of Co(III) porphyrins as NMR shift reagents for a range of ligand systems.[6−8] An interesting, recent development with analytical applications is the use of chiral Co(III) porphyrins as enantioselective receptors for amino acids, their esters, and other chiral ligands. Marchon and co-workers have, for example, shown that selective binding of mainly one enantiomer from a racemic mixture of a chiral ligand is possible when a chiral Co(III) porphyrin receptor is used.[2,3]

Our interest in bis(amine) complexes of Co(III) porphyrins stems from our work on the isoelectronic d^6 Fe(II) complexes[9] and fundamental questions which relate to the role of the N-terminal amino group of Tyr-1 in the plant cytochromes-*f*[10,11] as an axial ligand to the heme iron. In the case of Co(III) porphyrins, the coordination of amine ligands has been studied mainly by ^{1}H NMR spectroscopy,[12−14] particularly since these kinetically inert diamagnetic complexes are useful as NMR shift reagents.[6−8,15,16] Although X-ray structures of [Co(TPP)(Pip)](NO_3),[17,18] [Co(TPP)($PhCH(CH_3)NH_2$)$_2$]Br,[19] [Co(TMCP)((*R*/

* To whom correspondence should be addressed. E-mail: MunroO@nu.ac.za.

(1) Gouedard, M.; Gaudemer, F.; Gaudemer, A.; Riche, C. *J. Chem. Res., Synop.* **1978**, 30−31.
(2) Simonato, J.-P., Pécaut, J.; Marchon, J.-C. *J. Am. Chem. Soc.* **1998**, *120*, 7363−7364.
(3) Toronto, D.; Sarrazin, F.; Pécaut, J.; Marchon, J.-C.; Shang, M.; Scheidt, W. R. *Inorg. Chem.* **1998**, *37*, 526−532.
(4) Riche, C.; Gouedard, M.; Gaudemer, A. *J. Chem. Res., Synop.* **1978**, 34−35.
(5) Abraham, R. J.; Marsden, I. *Tetrahedron* **1992**, *48*, 7489−7504.
(6) Abraham, R. J.; Medforth, C. *J. Magn. Res. Chem.* **1990**, *28*, 343.
(7) Abraham, R. J.; Medforth, C. *J. Magn. Res. Chem.* **1988**, *26*, 803.
(8) Abraham, R. J.; Medforth, C. J. *J. Chem. Soc., Chem. Commun.* **1987**, 1637−1638.
(9) Munro, O. Q.; Madlala, P. S.; Warby, R. A. F.; Seda, T. B.; Hearne, G. *Inorg. Chem.* **1999**, *38*, 4724−4736.
(10) Martinez, S. E.; Huang, D.; Szczepaniak, A.; Cramer, W. A.; Smith, J. L. *Structure* **1994**, *2*, 95−105.
(11) Martinez, S. E.; Huang, D.; Ponomarev, M.; Cramer, W. A.; Smith, J. L. *Protein Sci.* **1996**, *5*, 1081−1092.
(12) Choi, I.-K.; Liu, Y.; Wei, Z.; Ryan, M. D. *Inorg. Chem.* **1997**, *36*, 3113−3118.
(13) Gouedard, M.; Gaudemer, F.; Gaudemer, A. *Tetrahedron Lett.* **1973**, 2257−2260.
(14) Mikros, E.; Gaudemer, F.; Gaudemer, A. *Inorg. Chem.* **1991**, *30*, 1806−1815.

10.1021/ic000976c CCC: $20.00
Published on Web 05/25/2001

S)-prolinol-N)$_2$]Cl,[2] and [Co(TMCP)((*S*)-2-butylamine)$_2$]Cl[3] have been reported, there have been no *systematic* structural, computational, and spectroscopic studies of a carefully tailored range of bis(amine) Co(III) porphyrin derivatives. The coordination chemistry, conformational energetics, electronic structures, and physical properties of this class of compounds have therefore not been fully delineated. Moreover, there have been no ^{59}Co NMR studies of bis(amine) complexes of Co(III) porphyrins, even though this technique has been applied to bis(imidazole)[20−22] and bis(pyridine)[23] complexes of Co(III) *meso*-tetraaryl porphyrins and is one of the few currently available direct experimental probes of the metal center.

In this paper, we present a general method for the synthesis of bis(amine) complexes of low-spin cobalt(III) porphyrins. Four complexes of the type [Co(TPP)(L)$_2$](SbF$_6$), where L = benzylamine, 1-butylamine, phenethylamine, and 1-methylpiperazine, have been characterized by X-ray crystallography as well as electronic, IR, and NMR (^{1}H, ^{13}C, and ^{59}Co) spectroscopy. Moreover, together with the atomic coordinates of [Co(TPP)(Pip)](NO$_3$),[18] the four X-ray structures of this study have been used to parametrize a force field (MM+) for bis(amine) derivatives of Co(III) porphyrins. The conformational energetics of these complexes have been determined by a combination of conventional dihedral angle mapping and MD simulations at 298 K. The force field has also been used to calculate accurate input geometries for DFT calculations of the electronic structures of a range of [Co(TPP)(amine)$_2$]$^+$ complexes. Importantly, this is the first report on the use of MM, MD, and DFT methods to delineate the fundamental factors which determine ^{59}Co chemical shifts and line widths in Co(III) porphyrins. We have found that the total 3d electron populations or, more fundamentally, the radial expectation values $\langle r^{-3}\rangle_{3d}$ reflect the σ-donor strengths of the axial ligands coordinated to the Co(III) ion. Moreover, a linear correlation exists between the ^{59}Co NMR line width, $\omega_{1/2}$, and the square of the calculated valence electric field gradient, q_{val}^2, of the Co(III) ion.

Experimental Section

General Information. All manipulations were carried out under nitrogen using a double manifold vacuum line, Schlenkware, and cannula techniques. THF and hexane were distilled over sodium/benzophenone. Dichloromethane, pyrrole, benzylamine, 1-butylamine, phenethylamine, and 1-methylpiperazine (all from Aldrich) were distilled over CaH$_2$. Benzaldehyde (Merck) and silver hexafluoroantimonate(V) (Aldrich) were used as received. H$_2$TPP was synthesized using published procedures.[24] [Co(TPP)Cl] was prepared by metalation of H$_2$TPP with cobalt(II) chloride hydrate in refluxing DMF.[25]

Instrumentation. Electronic spectra were recorded with a Shimadzu UV-2101PC UV−vis scanning spectrophotometer using dry methylene chloride solutions containing 0.1−0.5 M amine in 1.0 and 0.1 cm path length cuvettes. Samples for IR spectroscopy were KBr mulls of polycrystalline material. FT-IR spectra were recorded with a Perkin-Elmer Spectrum One spectrometer (4 scans, spectral resolution = 1.0 cm^{-1}). Microanalytical data (3 measurements per sample) were obtained with a Perkin-Elmer CHN 2400 Elemental Analyzer. ^{1}H and ^{13}C NMR spectra of all [Co(TPP)(L)$_2$]SbF$_6$ species were recorded using saturated solutions in CDCl$_3$ with a 500 MHz Varian Unity Inova spectrometer equipped with an Oxford magnet (11.744 T). Standard ^{1}H and ^{13}C pulse sequences were used for 1D and 2D spectra. The probe and setting temperatures of the instrument were calibrated using the chemical shift difference between the methyl and hydroxyl resonances of methanol for variable-temperature work.[26] ^{59}Co NMR spectra were recorded for several [Co(TPP)(L)$_2$]Cl derivatives, where L = 1-butylamine, **5**, benzylamine, **6**, phenethylamine, **7**, piperidine, **8**, 1-methylpiperazine, **9**, diethylamine, **10**, and dibutylamine, **11**, as a function of temperature. Samples were prepared by dissolving ∼15−20 mg of [Co(TPP)Cl] in 300 μL of CDCl$_3$ in thin-walled 5-mm diameter NMR tubes prior to adding 300 μL of freshly distilled amine. A broad band probe with three separate frequencies (76.750 MHz, deuterium lock; 499.982 MHz, proton decoupler; and 119.533 MHz, ^{59}Co observation frequency) was used for all ^{59}Co NMR spectra. The ^{59}Co resonance frequency of a saturated solution of K$_3$[Co(CN)$_6$] in D$_2$O was used as an external reference (eq 1),

$$\delta_{^{59}Co} = \frac{(\nu_{measured} - \nu_{reference})}{118.068} + (\delta_{lock}^{sample} - \delta_{lock}^{reference}) \qquad (1)$$

where 118.068 MHz is the theoretical ^{59}Co resonance frequency at 11.744 T; δ_{lock}^{sample} and $\delta_{lock}^{reference}$ are the lock solvent frequencies of the sample (CDCl$_3$) and reference (D$_2$O), respectively.[27,28] A pulse width of 7.0 μs was used with an acquisition time of 0.5 s (full relaxation was, however, evident after 0.01 s in all cases) and a spectral window of 400 kHz. Between 5000 and 10 000 transients were accumulated into 64 000 data points. Spectral singlets were fit to a single Voigt amplitude function with a time index of 13.2, eq 2,

$$I = a_0 \int_{-\infty}^{\infty} \frac{\exp(-t^2)}{a_3^2 + \left(\frac{\nu_{obs} - a_1}{a_2} - t\right)^2} dt \times \left(\int_{-\infty}^{\infty} \frac{\exp(-t^2)}{a_3^2 + t^2} dt\right)^{-1} \qquad (2)$$

where the adjustable variables a_0, a_1, a_2, and a_3 are the amplitude, resonance frequency, line width, and line shape, respectively.[29] The quintet spectra obtained for **6** were fit to the sum of five Voigt amplitude functions with equivalent width and shape parameters. A linear background was used for all line shape analyses. Because both **10** and

(15) Gaudemer, A.; Gaudemer, F.; Merienne, C. *Org. Magn. Reson.* **1983**, *21*, 83.
(16) Abraham, R. J.; Bedford, G. R.; Wright, B. *Org. Magn. Reson.* **1983**, *21*, 637−642.
(17) Abbreviations: 1-BuNH$_2$, 1-butylamine; 1-MePipz, 1-methylpiperazine; 4σ, 4 standard deviations; BzNH$_2$, benzylamine; C$_a$, C$_b$, C$_m$, porphyrin *alpha*-, *beta*-, and *meso*-carbons; C$_p$ and C$_L$, phenyl and ligand carbons; CSA, chemical shift anisotropy; DFT, density functional theory; DMF, *N*,*N*-dimethylformamide; EFG, electric field gradient; L, ligand in general; MD, molecular dynamics; MM, molecular mechanics; N$_p$, porphinato nitrogen; N$_{ax}$, axial ligand nitrogen; |N$_p$|, |C$_a$|, |C$_b$|, and |C$_m$| are the mean absolute perpendicular displacements of the porphyrin nitrogens, α-, *β*-, and *meso*-carbons from the 24-atom porphyrin mean plane, respectively; PhCH$_2$CH$_2$NH$_2$, phenethylamine; Pip, piperidine; THF, tetrahydrofuran; TMCP, dianion of 5, 10, 15, 20-tetrakis(2-methoxycarbonyl-3,3-dimethylcyclopropyl)porphyrin; TPP, 5, 10, 15, 20-tetraphenylporphyrin dianion.
(18) Scheidt, W. R.; Cunningham, J. A.; Hoard, J. L. *J. Am. Chem. Soc.* **1973**, *95*, 8289−8294.
(19) Riche, C.; Chiaroni, A.; Gouedard, M.; Gaudemer, A. *J. Chem. Res., Synop.* **1978**, 32−33.
(20) Hagen, K. I.; Schwab, C. M.; Edwards, J. O.; Sweigart, D. A. *Inorg. Chem.* **1986**, *25*, 978−983.
(21) Hagen, K. I.; Schwab, C. M.; Edwards, J. O.; Jones, J. G.; Lawler, R. G.; Sweigart, D. A. *J. Am. Chem. Soc.* **1988**, *110*, 7024−7031.
(22) Bang, H.; Edwards, J. O.; Kim, J.; Lawler, R. G.; Reynolds, K.; Ryan, W. J.; Sweigart, D. A. *J. Am. Chem. Soc.* **1992**, *114*, 2843−2852.
(23) Medek, A.; Frydman, V.; Frydman, L. *J. Phys. Chem. B* **1997**, *101*, 8959−8966.
(24) Barnett, G. H.; Hudson, M. F.; Smith, K. M. *J. Chem. Soc., Perkin Trans. (1)* **1975**, 1401−1403.
(25) Adler, A. D.; Longo, F. R.; Kampas, F.; Kim, J. *J. Inorg. Nucl. Chem.* **1970**, *32*, 2443−2445.
(26) Braun, S.; Kalinowski, H.-O.; Berger, S. *150 and More Basic NMR Experiments*; Wiley-VCH: Weinheim, 1998; pp 136−139.
(27) Brevard, C.; Granger, P. *Handbook of High-Resolution Multinuclear NMR*; John Wiley & Sons: New York, 1981; p 43.
(28) The temperature-dependence of the ^{59}Co resonance frequency of K$_3$[Co(CN)$_6$], $\nu_{reference}$, was established so that the correction could be applied at all temperatures.
(29) The program PeakFit 4.0 (SPSS Inc., 444 N. Michigan Avenue, Chicago, IL 60611) was used for all line shape analyses. Equation 2 is written with integrals because the convolution integrals lack real closed form solutions. The analytical closed form complex solutions are, however, used during fitting to give exact Voigt functions to at least 14 significant figures.

11 showed some CSA[17] effects (slight to moderate line shape distortion), Voigt amplitude functions with variable width and shape parameters were used to fit the NMR data. The intrinsic line widths for these two derivatives were taken as the average width of the three (resolved) center lines of the quintet in each case.

Synthesis of [Co(TPP)(BzNH$_2$)$_2$](SbF$_6$), 1. To [Co(TPP)Cl] (100 mg, 0.15 mmol) and $AgSbF_6$ (58 mg, 0.17 mmol) in a two-neck 100-mL round-bottom flask under nitrogen was added 50 mL of freshly distilled THF. The solution was allowed to stir for ~24 h at room temperature prior to removing the solvent *in vacuo*. The red-brown solid, [Co(TPP)($FSbF_5$)], was redissolved in dichloromethane (~20 mL) and filtered under nitrogen. Addition of benzylamine (0.5 mL, 4.6 mmol) changed the solution from red-brown to purple on swirling. The solution was transferred (~2-mL aliquots) into ten 15 × 150 mm test tubes; each aliquot was layered with hexane. X-ray quality crystals were obtained after 5 days. Crystals of **1** were collected by filtration and washed with 40% ethanol in hexane to remove yellow-brown crystals of benzylamine. Isolated yield: 72 mg, 46%. Anal. Calcd for $C_{58}H_{46}N_6CoSbF_6$: C, 62.1; H, 4.1; N, 7.5. Found: C, 61.8; H, 3.7; N, 7.4. IR (KBr pellet): 3309 cm^{-1}, 3254 cm^{-1} (w, ν(N−H)), 1588 cm^{-1} (m, δ(NH_2)), 1165 cm^{-1} (m, ρ_t(NH_2)), 658 cm^{-1} (s, ν(Sb−F)). UV−vis (CH_2Cl_2) [λ_{max}, nm (ϵ, M^{-1}cm^{-1})]: 431 (238 × 10^3), 546 (12.2 × 10^3), 577 (5.71 × 10^3). ^{1}H NMR (499.98 MHz, $CDCl_3$) [δ, ppm]: 9.17 (s, 8H, pyrrole-H); 8.15 (d, ^3J = 7.0 Hz, 8H, TPP *o*-H); 7.80 (m, 12H, TPP *m*,*p*-H); 6.67 (t, ^3J = 7.7 Hz, 2H, $BzNH_2$ *p*-H); 6.46 (t, ^3J = 7.7 Hz, 4H, $BzNH_2$ *m*-H); 4.58 (d, ^3J = 7.7 Hz, 4H, $BzNH_2$ *o*-H); −2.78 (t, ^3J = 7.0 Hz, 4H, α-CH_2); −5.50 (t, ^3J = 7.0 Hz, 4H, NH_2). ^{13}C NMR (125.736 MHz, $CDCl_3$) [δ, ppm]: 41.62 (α-C, $BzNH_2$); 119.76 (C_m, TPP); 125.47 (*o*-C, $BzNH_2$); 127.28 (*m*-C, TPP); 127.53 (*p*-C, $BzNH_2$); 128.09 (*m*-C, $BzNH_2$); 128.45 (*p*-C, TPP); 133.53 (β-C, $BzNH_2$); 134.18 (*o*-C, TPP); 135.48 (C_b, TPP); 140.09 (C_{phenyl}−C_m, TPP); 143.47 (C_a, TPP).

Synthesis of [Co(TPP)(1-BuNH$_2$)$_2$](SbF$_6$), 2. A similar procedure to that described above was employed using [Co(TPP)Cl] (100 mg, 0.15 mmol), $AgSbF_6$ (74 mg, 0.22 mmol), and 1-butylamine (300 μL, 2.9 mmol). The reaction mixture was transferred in equal aliquots to four 25 × 180 mm Schlenk tubes and layered with hexane. X-ray quality crystals were obtained from the CH_2Cl_2/hexane mixture after 4 days. Isolated yield: 77.6 mg, 50%. Anal. Calcd for $C_{52}H_{50}N_6CoSbF_6$: C, 59.3; H, 4.8; N, 8.0. Found: C, 59.2; H, 4.7; N, 7.8. IR (KBr pellet): 3302 cm^{-1}, 3258 cm^{-1} (w, ν(N−H)), 1584 cm^{-1} (m, δ(NH_2)), 1100 cm^{-1} (m, ρ_t(NH_2)), 655 cm^{-1} (s, ν(Sb−F)). UV−vis (CH_2Cl_2) [λ_{max}, nm (ϵ, M^{-1}cm^{-1})]: 430 (534 × 10^3), 545 (24.1 × 10^3), 580 (10.1 × 10^3). ^{1}H NMR (499.98 MHz, $CDCl_3$) [δ, ppm]: 9.18 (s, 8H, pyrrole-H); 8.17 (dd, ^3J = 7.4 Hz, ^4J = 1.7 Hz, 8H, *o*-H); 7.80 (m, 12H, *m*,*p*-H); −0.37 (t, ^3J = 7.4 Hz, 6H, CH_3); −0.89 (m, 4H, γ-CH_2); −1.66 (m, 4H, β-CH_2); −4.00 (m, 4H, α-CH_2); −5.93 (t, ^3J = 5.8 Hz, 4H, NH_2). ^{13}C NMR (125.736 MHz, $CDCl_3$) [δ, ppm]: 11.90 (δ-C, 1-$BuNH_2$); 17.48 (γ-C, 1-$BuNH_2$); 28.64 (β-C, 1-$BuNH_2$); 37.10 (α-C, 1-$BuNH_2$); 119.93 (C_m, TPP); 127.24 (*m*-C, TPP); 128.41 (*p*-C, TPP); 134.22 (*o*-C, TPP); 135.18 (C_b, TPP); 140.40 (C_{phenyl}−C_m, TPP); 143.73 (C_a, TPP).

Synthesis of [Co(TPP)(PhCH$_2$CH$_2$NH$_2$)$_2$](SbF$_6$), 3. [Co(TPP)Cl] (100 mg, 0.15 mmol), $AgSbF_6$ (142 mg, 0.41 mmol), and phenethylamine (400 μL, 3.2 mmol) were reacted as described above. Test tubes (15 × 150 mm) were used for crystallization; X-ray quality crystals were obtained from CH_2Cl_2/hexane after 5 days. Isolated yield: 126.4 mg, 75%. Anal. Calcd for $C_{60}H_{50}N_6CoSbF_6$: C, 62.7; H, 4.4; N, 7.3. Found: C, 62.3; H, 4.2; N, 7.2. IR (KBr pellet): 3307 cm^{-1}, 3252 cm^{-1} (w, ν(N−H)), 1587 cm^{-1} (m, δ(NH_2)), 1145 cm^{-1} (m, ρ_t(NH_2)), 654 cm^{-1} (s, ν(Sb−F)). UV−vis (CH_2Cl_2) [λ_{max}, nm (ϵ, M^{-1}cm^{-1})]: 429 (363 × 10^3), 544 (17.3 × 10^3), 577 (8.67 × 10^3). ^{1}H NMR (499.98 MHz, $CDCl_3$) [δ, ppm]: 9.13 (s, 8H, pyrrole-H); 8.08 (dd, ^3J = 6.6 Hz, ^4J = 1.7 Hz, 8H, *o*-H); 7.80 (m, 12H, *m*,*p*-H); 6.81 (t, ^3J = 7.4 Hz, 2H, $PhCH_2CH_2NH_2$ *p*-H); 6.64 (t, ^3J = 7.8 Hz, 4H, $PhCH_2CH_2NH_2$ *m*-H); 5.08 (d, ^3J = 7.0 Hz, 4H, $PhCH_2CH_2NH_2$ *o*-H); −0.23 (t, ^3J = 6.6 Hz, 4H, β-CH_2); −3.74 (t, ^3J = 7.0 Hz, 4H, α-CH_2); −5.99 (t, ^3J = 6.2 Hz, 4H, NH_2). ^{13}C NMR (125.736 MHz, $CDCl_3$) [δ, ppm]: 32.07 (β-C, $PhCH_2CH_2NH_2$); 37.83 (α-C, $PhCH_2CH_2NH_2$); 119.98 (C_m, TPP); 126.23 (*p*-C, $PhCH_2CH_2NH_2$); 126.54 (*o*-C, $PhCH_2CH_2NH_2$); 127.11 (*m*-C, TPP); 128.12 (*m*-C, $PhCH_2CH_2NH_2$); 128.37 (*p*-C, TPP); 134.29 (*o*-C, TPP); 134.41 (γ-C, $PhCH_2CH_2NH_2$); 135.08 (C_b, TPP); 140.35 (C_{phenyl}−C_m, TPP); 143.77 (C_a, TPP).

Synthesis of [Co(TPP)(1-MePipz)$_2$](SbF$_6$), 4. [Co(TPP)Cl] (100 mg, 0.15 mmol), $AgSbF_6$ (224 mg, 0.65 mmol), and 1-methylpiperazine (330 μL, 3.0 mmol) were reacted as described above. X-ray quality crystals of the monohydrate, [Co(TPP)(1-MePipz)$_2$](SbF_6)·H_2O, were grown from CH_2Cl_2/hexane over a period of 5 days in five 15 × 150 mm test tubes. Isolated yield: 53 mg, 32%. Anal. Calcd for $C_{54}H_{54}N_6OCoSbF_6$: C, 57.6; H, 4.8; N, 10.0. Found: C, 57.1; H, 4.6; N, 9.8. IR (KBr pellet): 3234 cm^{-1} (w, ν(N−H)), 660 cm^{-1} (s, ν(Sb−F)). UV−vis (CH_2Cl_2) [λ_{max}, nm (ϵ, M^{-1}cm^{-1})]: 430 (266 × 10^3), 544 (12.6 × 10^3), 578 (5.48 × 10^3). ^{1}H NMR (499.98 MHz, $CDCl_3$) [δ, ppm]: 9.24 (s, 8H, pyrrole-H); 8.19 (dd, ^3J = 7.6 Hz, ^4J = 1.7 Hz, 8H, TPP *o*-H); 7.83 (m, 12H, TPP *m*,*p*-H); 0.94 (s, 6H, N−CH_3); 0.44 (d, J = 13.4 Hz, 4H, β-CH_2); −0.98 (t, J = 11.8 Hz, 4H, β-CH_2); −3.76 (m, 4H, α-CH_2); −4.52 (d, J = 12.6 Hz, 4H, α-CH_2); −6.89 (t, ^3J = 11.8 Hz, 2H, NH). ^{13}C NMR (125.736 MHz, $CDCl_3$) [δ, ppm]: 43.83 (N−CH_3, 1-MePipz); 43.93 (β-C, 1-MePipz); 53.25 (α-C, 1-MePipz); 120.40 (C_m, TPP); 127.44 (*m*-C, TPP); 128.77 (*p*-C, TPP); 134.34 (*o*-C, TPP); 135.86 (C_b, TPP); 139.73 (C_{phenyl}−C_m, TPP); 143.77 (C_a, TPP).

X-ray Structure Determinations. Intensity measurements were made on air-stable crystals of compounds **1**−**4** that were platelike lustrous purple rhombs with the approximate dimensions 0.6 × 0.5 × 0.4 mm^3, 0.6 × 0.5 × 0.2 mm^3, 0.4 × 0.4 × 0.3 mm^3, and 0.8 × 0.3 × 0.2 mm^3 (needlelike), respectively. The X-ray diffraction data were collected with a Siemens SMART 1000 CCD area detector diffractometer at −100 °C with graphite-monochromated Mo Kα radiation ($\bar{\lambda}$ = 0.71703 Å). Data were corrected for Lorentz and polarization factors but not for absorption (μ ~0.9 mm^{-1} for all four compounds). A total of 28 493, 46 199, 28 353, and 50 381 observed reflections ($F_o \geq 2.0\sigma(F_o)$) were collected and averaged to 5760, 5947, 12 360, and 12 264 unique reflections for **1**−**4**, respectively.

Direct methods (SHELXS-97, OSCAIL V8)[30,31] were used to solve the structures of **1** and **2** in the orthorhombic space group *Pbcn*. The structures of **3** and **4** were similarly solved in the monoclinic space groups $P2_1$ and $P2_1/c$, respectively. Difference Fourier syntheses were used to locate the remaining non-hydrogen atoms in each case. The structures were refined anisotropically against F^2 with SHELXL-97.[32] A final difference Fourier synthesis for **1** located all of the hydrogens atoms, including those of the coordinated amine nitrogens. In the case of **2**, the final difference Fourier synthesis located most of the hydrogen atoms and indicated that the axial ligand methyl group (C(34)) was disordered about two positions. The latter were refined as separate parts to a final site occupancy factor of 0.718. In the case of **3**, the final difference Fourier synthesis located all of the porphyrin hydrogens and suggested that one of the axial phenethylamine ligands had two conformations that were related by a 43.3° rotation about the Co−N(6) bond (measured by the N(1)−Co−N(6)−C(61) dihedral angle). Both conformations were refined as separate parts (the final dihedral angle between the disordered phenyl groups measured 21.1(9)°) to a final site occupancy factor of 0.527. The absolute configuration of **3** could not be determined unambiguously from the value of the Flack parameter.[33] The final difference Fourier synthesis for **4** located all of the porphyrin hydrogens as well as an oxygen atom of a water molecule 2.93 Å from the methylated nitrogen, N(6), of one of the axial 1-methylpiperazine ligands. With the exception of the hydrogen atoms belonging to the solvate water of **4**, all hydrogen atoms for the four structures were included as idealized contributors in the least-squares process with standard SHELXL-97 idealization parameters. The final refinements converged to the discrepancy indices listed below. The maximum (and minimum) electron densities on the final difference Fourier maps of **1**−**4** were 0.446 (−0.623), 0.590 (−0.645), 0.350 (−0.475), and 2.541 (−1.311) e/Å^3, respectively. The maximum residual electron density peak, Q(1), of 2.541 e/Å^3 in the difference Fourier map of **4** was located 1.14 Å from N(6) and 2.00 Å from the oxygen

(30) Sheldrick, G. M. *Acta Crystallogr., Sect. A* **1990**, *A46*, 467−473.
(31) McArdle, P. *J. Appl. Crystallogr.* **1995**, *28*, 65.
(32) Sheldrick, G. M.; Schneider, T. R. *Methods Enzymol.* **1997**, *277*, 319−343.
(33) Flack, H. D. *Acta Crystallogr., Sect. A* **1983**, *A39*, 876−881.

atom, O(1), of the water molecule H-bonded to N(6). Since the angles C(52)−N(6)−Q(1) (102.7°) and C(53)−N(6)−Q(1) (139.5°) were inconsistent with those for an sp^3-hybridized quaternary nitrogen (e.g., a protonated nitrogen), the peak was not assigned to any specific atom.

Complete crystallographic details, fractional atomic coordinates for all non-hydrogen atoms, anisotropic thermal parameters, fixed hydrogen atom coordinates, bond lengths, bond angles, and dihedral angles for compounds **1**−**4** are given in the Supporting Information (Tables S1−S28). Experimental lattice constants and SHELXL-97 refinement parameters for the four compounds are given below.

[Co(TPP)(BzNH$_2$)$_2$](SbF$_6$). $C_{58}H_{46}N_6CoSbF_6$, fw = 1121.69 amu, a = 17.0323(8) Å, b = 12.2935(6) Å, c = 23.4079(11) Å, V = 4901.3(4) Å^3, orthorhombic, *Pbcn*, Z = 4, D_c = 1.520 g cm^{-3}, μ = 0.959 mm^{-1}, T = 173(2) K, R_1 (wR_2)[34] = 0.0342 (0.0759) for 4922 unique data with $I > 2\sigma(I)$, R_1 (wR_2) = 0.0433 (0.0803) for all 5760 data (R_{int} = 0.0347).

[Co(TPP)(1-BuNH$_2$)$_2$](SbF$_6$). $C_{52}H_{50}N_6CoSbF_6$, fw = 1053.66 amu, a = 16.2614(9) Å, b = 12.7546(7) Å, c = 23.2873(12) Å, V = 4830.0(5) Å^3, orthorhombic, *Pbcn*, Z = 4, D_c = 1.449 g cm^{-3}, μ = 0.968 mm^{-1}, T = 173(2) K, R_1 (wR_2)[34] = 0.0593 (0.0857) for 4579 unique data with $I > 2\sigma(I)$, R_1 (wR_2) = 0.0868 (0.0930) for all 5947 data (R_{int} = 0.0725).

[Co(TPP)(PhCH$_2$CH$_2$NH$_2$)$_2$](SbF$_6$). $C_{60}H_{50}N_6CoSbF_6$, fw = 1149.74 amu, a = 10.6378(5) Å, b = 22.0466(11) Å, c = 10.9585(5) Å, β = 94.2140(10)°, V = 2563.1(2) Å^3, monoclinic, *P*2$_1$, Z = 2, D_c = 1.490 g cm^{-3}, μ = 0.919 mm^{-1}, T = 173(2) K, R_1 (wR_2)[34] = 0.0334 (0.0708) for 11393 unique data with $I > 2\sigma(I)$, R_1 (wR_2) = 0.0388 (0.0746) for all 12360 data (R_{int} = 0.0255).

[Co(TPP)(1-MePipz)$_2$](SbF$_6$)·H$_2$O. $C_{54}H_{54}N_8OCoSbF_6$, fw = 1125.70 amu, solvent/asymmetric unit = H_2O, a = 13.4112(9) Å, b = 19.0611(12) Å, c = 19.6630(13) Å, β = 93.2450(10)°, V = 5018.4(6) Å^3, monoclinic, *P*2$_1$/*c*, Z = 4, D_c = 1.487 g cm^{-3}, μ = 0.939 mm^{-1}, T = 173(2) K, R_1 (wR_2)[34] = 0.0951 (0.2360) for 7271 unique data with $I > 2\sigma(I)$, R_1 (wR_2) = 0.1547 (0.2759) for all 12264 data (R_{int} = 0.0868).

Molecular Mechanics Calculations. HyperChem 5.02 (MM+ force field)[35] was used for all calculations. Porphyrin core parameters were taken from our published force field for iron porphyrins.[36−38] New bond stretching, angle bending, and dihedral angle parameters for bis(amine) cobalt(III) derivatives were developed by fitting the structures of **1**−**4** and [Co(TPP)(Pip)$_2$](NO$_3$),[18] calculated in the presence of all lattice neighbors, to their X-ray structures.[39] A root-mean-square gradient termination cutoff of 0.005 kcal/(Å mol) was used for geometry optimization with the Polak−Ribiere conjugate gradient algorithm. A dielectric constant of 1.5 D was employed for all calculations. The vacuum dielectric constant (1.0 D) was not used because even in the gas-phase some screening of intramolecular dipole−dipole interactions occurs.[40,41] Partial atomic charges were not included in the calculations.[38,42,43] Conformational surfaces for [Co(TPP)(1-BuNH$_2$)$_2$]$^+$, [Co(TPP)(1-MePipz)$_2$]$^+$, and [Co(TPP)(Et$_2$NH)$_2$]$^+$ were calculated as described previously.[9]

Molecular Dynamics Simulations. HyperChem 5.02 was used for gas-phase MD simulations of [Co(TPP)(1-BuNH$_2$)$_2$]$^+$, [Co(TPP)(BzNH$_2$)$_2$]$^+$, [Co(TPP)(PhCH$_2$CH$_2$NH$_2$)$_2$]$^+$, [Co(TPP)(1-MePipz)$_2$]$^+$, and [Co(TPP)(Et$_2$NH)$_2$]$^+$ at a constant temperature of 298 K with a bath relaxation constant of 0.1 ps. A heating time of 10 ps was used to heat the system from 0 to 298 K in 5 K increments. This was followed by a 500 ps simulation interval at the set temperature employing 0.5 fs time steps. Data were collected at 7.5 fs intervals, affording 6.8 × 10^4 snapshots. At least four simulations, starting from unique input coordinates, were used to check the generality of the results in each case. The data were reduced for plotting by using a 75 fs sampling interval for the analysis of each MD trajectory.

DFT Calculations. DFT calculations (pseudospectral method,[44] B3LYP functional,[45] LACVP basis set,[46] medium grid) were performed with Jaguar 4.0[47] running on a Compaq AlphaStation DS20e. The LACVP basis set employs effective core potentials for the elements K−Cu, Rb−Ag, Cs−La, and Hf−Au. Second and third row s- and p-block elements are described by Pople's 6-31G[48] basis set. Input coordinates for all [Co(TPP)(L)$_2$]$^+$ cations were energy minima obtained from MM geometry optimizations in the gas phase. In the case of [Co(TPP)Cl], the X-ray coordinates[49] were used as a starting structure for a full geometry optimization at the B3LYP/LACVP level of theory. The converged DFT wave functions for each complex were analyzed with Weinhold's NBO 4.M program[50] which uses the first-order reduced density matrix of the wave function to obtain natural atomic orbitals (NAOs) and natural electron populations for the system.

Results

Crystal Structures. The molecular structures of **2** and **4** are shown in the ORTEP[51] plots of Figure 1. Formal diagrams of the porphinato cores of the two derivatives are shown in Figure 2; the perpendicular displacement of each crystallographically

(34) $R_1 = \sum||F_o| - |F_c||/\sum|F_o|$ and $wR_2 = \{\sum[w(F_o^2 - F_c^2)^2]/\sum[wF_o^4]\}^{1/2}$. R factors R_1 are based on F, with F set to zero for negative F^2. The criterion of $F^2 > 2\sigma(F^2)$ was used only for calculating R_1. R factors based on F^2 (wR_2) are statistically about twice as large as those based on F.

(35) *HyperChem*, version 5.02: Hypercube, Inc.: Gainsville, FL.

(36) Munro, O. Q.; Bradley, J. C.; Hancock, R. D.; Marques, H. M.; Marsicano, F.; Wade, P. W. *J. Am. Chem. Soc.* **1992**, *114*, 7218−7230.

(37) Marques, H. M.; Munro, O. Q.; Grimmer, N. E.; Levendis, D. C.; Marsicano, F.; Pattrick, G.; Markoulides, T. *J. Chem. Soc., Faraday Trans.* **1995**, *91*, 1741−1749.

(38) Munro, O. Q.; Marques, H. M.; Debrunner, P. G.; Mohanrao, K.; Scheidt, W. R. *J. Am. Chem. Soc.* **1995**, *117*, 935−954.

(39) The following parameters were developed for bis(amine) Co(III) porphyrins using the X-ray structures of **1**−**4** and [Co(TPP)(Pip)$_2$](NO$_3$)[18] for parametrization. Bond deformation: bond, k_s (mdyn Å^{-1}), l_0 (Å); N_p−Co(III), 2.000, 1.892; N_{ax}−Co(III), 2.650, 1.927. Bond angle deformation: angle, k_θ (mdyn Å rad^{-2}), θ_0 (deg); *trans*-N_p−Co(III)−N_p, 0.005, 180.0; *cis*-N_p−Co(III)−N_p, 0.200, 90.0; N_p−Co(III)−N_{ax}, 1.250, 90.0; N_{ax}−Co(III)−N_{ax}, 1.000, 180.0; C_a−N_p−Co(III), 0.700, 126.8; C(sp^3)−N_{ax}−Co(III), 0.600, 124.0; H−N_{ax}−Co(III), 0.400, 109.47; C(sp^3)−N_{ax}−C(sp^3), 0.630, 111.7. Dihedral angle deformation: dihedral angle, V_1, V_2, V_3 (kcal mol^{-1}); C_a−N_p−Co(III)−N_p (N_p−Co(III)−N_p trans), 0.000, 0.000, 0.000; C_a−N_p−Co(III)−N_p (N_p−Co(III)−N_p cis), 0.000, 0.100, 0.000; Co(III)−N_{ax}−C(sp^3)−H, 0.000, 0.000, 0.520; Co(III)−N_{ax}−C(sp^3)−C(sp^3), −0.200, 0.730, 0.800; Co(III)−N_{ax}−C(sp^3)−C(sp^2), 0.000, 0.000, 0.000; N_p−Co(III)−N_{ax}−C(sp^3), 0.000, 0.000, 0.000; N_p−Co(III)−N_{ax}−H, 0.000, 0.000, 0.000; N_{ax}−Co(III)−N_{ax}−H, 0.000, 0.000, 0.000; C(sp^2)−C(sp^2)−C(sp^3)−N_{ax}, 0.000, 0.000, 0.000; C_b−C_a−N_p−Co(III), 0.000, 0.100, 0.000; C_m−C_a−N_p−Co(III), 0.000, 0.200, 0.000. Out-of-plane deformation: sp^2-hybridized−attached atom, k_{oop} (mdyn Å rad^{-2}); N_p−Co(III), 0.050; C_a−N_p, 0.050.

(40) (a) Allinger, N. L. *J. Am. Chem. Soc.* **1977**, *99*, 8127. (b) Allinger, N. L.; Yuh, Y. MM2(87). Distributed to academic users by QCPE, under special agreement with Molecular Design Ltd., San Leandro, CA. (c) Sprague, J. T.; Tai, J. C.; Young, Y.; Allinger, N. L. *J. Comput. Chem.* **1987**, *8*, 581.

(41) Jensen, F. Introduction to Computational Chemistry; Wiley: New York, 1999; pp 23−25.

(42) Shelnutt, J. A.; Medforth, C. J.; Berber, M. D.; Barkigia, K. M.; Smith, K. M. *J. Am. Chem. Soc.* **1991**, *113*, 4077−4087.

(43) The force field includes the standard MM2[40] bond dipoles for the C−C and C−N bonds. All M−L bond dipoles have an assigned value of zero.

(44) Jaguar[47] solves the Schrödinger equation iteratively using SCF methods to calculate the lowest-energy wave function within the space spanned by the basis set. The fundamental integrals are, however, computed in physical space on a grid rather than in the spectral space defined by the basis functions, affording a sizable speed increase for large systems. (a) Friesner, R. A. *Chem. Phys. Lett.* **1985**, *116*, 39. (b) Friesner, R. A. *Annu. Rev. Phys. Chem.* **1991**, *42*, 341.

(45) Becke, A. D. *J. Chem. Phys.* **1993**, *98*, 5648.

(46) Hay, P. J.; Wadt, W. R. *J. Chem. Phys.* **1985**, *82*, 299−310.

(47) *Jaguar*, version 4.0; Schrödinger, Inc.: Portland, OR, 2000.

(48) (a) Rassolov, V. A.; Pople, J. A.; Ratner, M. A.; Windus, T. L. *J. Chem. Phys.* **1998**, *109*, 1223. (b) Francl, M. M.; Pietro, W. J.; Hehre, W. J.; Binkley, J. S.; Gordon, M. S.; DeFrees, D. J.; Pople, J. A. *J. Chem. Phys.* **1982**, *77*, 3654−3665.

(49) Sakurai, T.; Yamamoto, K.; Naito, H.; Nakamoto, N. *Bull. Chem. Soc. Jpn.* **1976**, *49*, 3042−3046.

(50) Glendening, E. D.; Badenhoop, J. K.; Reed, A. E.; Carpenter, J. E.; Weinhold, F. *NBO 4.M*; Theoretical Chemistry Institute, University of Wisconsin: Madison, WI, 1999.

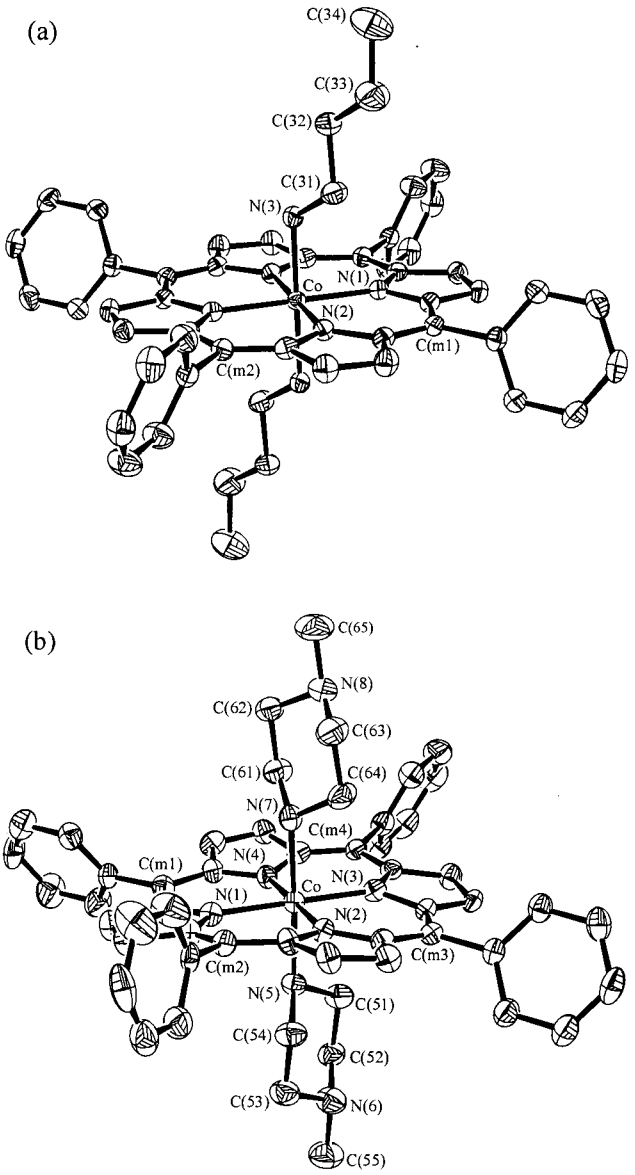

Figure 1. ORTEP diagrams (displaying selected atom labels) of the low-temperature X-ray structures (−100 °C) of (a) $[Co(TPP)(1\text{-}BuNH_2)_2](SbF_6)$ and (b) $[Co(TPP)(1\text{-}MePipz)_2](SbF_6)\cdot H_2O$. Thermal ellipsoids are drawn at the 50% probability level. Hydrogen atoms, SbF_6^- anions, and a solvent water molecule in (b) have been omitted for clarity.

unique atom from the 24-atom porphyrin mean plane and the averaged values of the chemically unique bond distances and angles are displayed in each case. The orientations of the axial ligands relative to the Co−N_p bonds are also shown. (Selected bond distances and angles for compounds **1**−**4** are given in Table 1; the average *absolute* perpendicular displacements of the chemically unique atoms of the porphyrin core from the 24-atom mean plane are given in Table 2.) ORTEP plots and formal diagrams of the porphinato cores of **1** and **3** are given in the Supporting Information (Figures S1 and S2, respectively). Complete listings of structural data (bond lengths, bond angles, and dihedral angles) for compounds **1**−**4** are given in the Supporting Information (Tables S3−S5, S10−S12, S17−S19, and S24−S26).

(51) *ORTEP-3 for Windows*, v1.05. (Farrugia, L. J. *J. Appl. Crystallogr.* **1997**, *30*, 565.) This program is based on *ORTEP-III*, v1.02. (Burnett, M. N.; Johnson, C. K. Oak Ridge National Laboratory report ORNL-6895, 1996.)

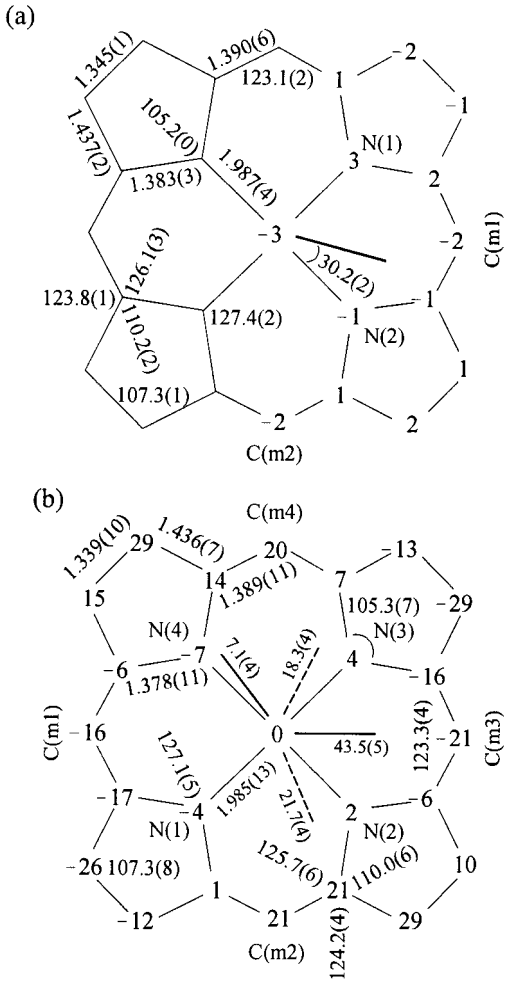

Figure 2. Formal diagrams of the porphyrin cores of (a) $[Co(TPP)(1\text{-}BuNH_2)_2](SbF_6)$ and (b) $[Co(TPP)(1\text{-}MePipz)_2](SbF_6)\cdot H_2O$. Averaged values (and their esd's) of the chemically unique bond distances (in Å) and angles (in degrees) are shown. The perpendicular displacements (in units of 0.01 Å) of the cobalt and 24 porphyrin core atoms from the porphyrin mean plane are also displayed. The dihedral angles (deg) of the axial ligands (N_p−Co−N_{ax}−C_α) are indicated by the solid and dashed lines for the above- and below-plane ligands, respectively.

The crystal structure of **2** is centrosymmetric and, to a large extent, representative of the conformations of the three bis(1° amine) derivatives of this study; each has a relatively planar porphyrin core conformation (Figures 2 and S2) and axial amine orientations that reflect either the crystallographically required center of inversion at the cobalt(III) ion or, in the case of **3**, an approximately centrosymmetric *cation*. The Co−N_{ax} distance in **2** is 1.980(2) Å; the Co−N_p distances average to 1.987(4) Å. The butylamine ligands exhibit an anti arrangement with a symmetry-unique orientation of 30.2(2)° relative to the nearest Co−N_p vector (N(2)−Co−N(3)−C(31) dihedral angle). The two Co−N_{ax} vectors are slightly canted from the heme normal with individual N_p−Co−N(3) angles spanning the range 88.2(1)−91.8(1)°. The Co−N(3)−C(31) angle measures 121.0(2)°. The dihedral angles between the phenyl rings appended to C(m1) and C(m2) and the 24-atom porphyrin mean plane are 69.4(1)° and 73.3(1)°, respectively. As noted above, the structure of **2** is exemplary of the bis(1° amine) derivatives; the rather similar coordination group distances and angles for **1** and **3** are therefore given in Table 1 without further comment. One noteworthy difference between the structure of **2** and the structures of compounds **1** and **3** is the absence of H-bonding interactions between the SbF_6^- anion and the axial ligand NH_2 protons. As

Table 1. Selected Bond Lengths and Bond Angles for $[Co(TPP)(1\text{-}BuNH_2)_2](SbF_6)$, $[Co(TPP)(BzNH_2)_2](SbF_6)$, $[Co(TPP)(PhCH_2CH_2NH_2)_2](SbF_6)$, and $[Co(TPP)(1\text{-}MePipz)_2](SbF_6)\cdot H_2O$

	$[Co(P)(L^1)_2]X^{a,b}$	$[Co(P)(L^2)_2]X^{a,c}$		$[Co(P)(L^3)_2]X^{a,d}$	$[Co(P)(L^4)_2]X^{a,e}$
		(A) bond lengths (Å)[f]			
Co−N(1)	1.995(2)	1.989(2)	Co−N(1)	1.986(2)	1.994(5)
Co−N(2)	1.979(2)	1.984(2)	Co−N(2)	1.988(2)	1.976(4)
Co−N(3)	1.983(2)	1.980(2)	Co−N(3)	1.982(2)	1.971(4)
			Co−N(4)	1.986(2)	1.997(5)
			Co−N(5)	1.972(2)	2.039(5)
			Co−N(6)[h]	1.983(2)	2.041(5)
		(B) bond angles (deg)[f]			
N(1)−Co−N(1)[g]	180.0(0)	180.0(1)	N(3)−Co−N(1)	179.8(1)	179.7(2)
N(2)−Co−N(2)[g]	180.0(0)	180.0(1)	N(4)−Co−N(2)	179.8(1)	178.7(2)
N(3)−Co−N(3)[g]	180.0(0)	180.0(2)	N(5)−Co−N(6)[h]	179.4(1)	177.5(2)
N(2)−Co−N(3)	88.7(1)	91.8(1)	N(5)−Co−N(3)	94.0(1)	91.3(2)
N(2)[g]−Co−N(3)	91.3(1)	88.2(1)	N(3)−Co−N(6)[h]	86.1(1)	91.1(2)
N(2)−Co−N(3)[g]	91.3(1)	88.2(1)	N(5)−Co−N(1)	85.9(1)	88.5(2)
N(2)[g]−Co−N(3)[g]	88.7(1)	91.8(1)	N(6)[h]−Co−N(1)	94.0(1)	89.1(2)
N(2)−Co−N(1)	89.8(1)	90.1(1)	N(5)−Co−N(4)	90.0(1)	87.5(2)
N(2)[g]−Co−N(1)	90.2(1)	89.9(1)	N(3)−Co−N(4)	89.9(1)	90.2(2)
N(2)−Co−N(1)[g]	90.2(1)	89.9(1)	N(6)[h]−Co−N(4)	89.4(1)	92.2(2)
N(2)[g]−Co−N(1)[g]	89.8(1)	90.1(1)	N(1)−Co−N(4)	90.3(1)	90.1(2)
N(3)−Co−N(1)	91.3(1)	90.4(1)	N(5)−Co−N(2)	89.9(1)	91.3(2)
N(3)[g]−Co−N(1)	88.7(1)	89.6(1)	N(3)−Co−N(2)	90.1(1)	89.6(2)
N(3)−Co−N(1)[g]	88.7(1)	89.6(1)	N(6)[h]−Co−N(2)	90.7(1)	89.1(2)
N(3)[g]−Co−N(1)[g]	89.8(1)	90.4(1)	N(1)−Co−N(2)	89.7(1)	90.1(2)

[a] X = SbF_6, P = TPP. [b] L^1 = benzylamine. [c] L^2 = 1-butylamine. [d] L^3 = phenethylamine. [e] L^4 = 1-methylpiperazine. [f] The estimated standard deviations of the least significant digits are given in parentheses. [g] Symmetry equivalent $(-x,-y,-z)$. [h] N(7) in the case of $[Co(TPP)(1\text{-}MePipz)_2](SbF_6)\cdot H_2O$.

Table 2. Selected Crystallographic and MM-Calculated Conformational Data for Bis(amine)(*meso*-tetraphenylporphinato)Co(III) Derivatives

	$[Co(TPP)(L^1)_2]X^a$			$[Co(TPP)(L^2)_2]X^a$			$[Co(TPP)(L^3)_2]X^a$			$[Co(TPP)(L^4)_2]X\cdot H_2O^a$			$[Co(TPP)(L^5)_2]Y\cdot Pip^a$		
	X-ray	lattice[b]	gas[c]	X-ray	lattice[b]	gas[c]	X-ray	lattice[b]	gas[c]	X-ray	lattice[b]	gas[c]	X-ray[d]	lattice[b]	gas[c]
$Co-N_{ax}$[e]	1.980(2)	1.976(0)	1.971(0)	1.983(2)	1.978(0)	1.969(0)	1.978(8)	1.975(1)	1.984(0)	2.040(1)	2.054(4)	2.028(0)	2.060(3)	2.061(2)	2.047(0)
$Co-N_p$[f]	1.987(4)	1.988(5)	1.986(3)	1.987(11)	1.986(5)	1.986(3)	1.986(3)	1.987(3)	1.987(4)	1.985(13)	1.982(7)	1.973(3)	1.979(6)	1.987(4)	1.987(0)
ϕ[g]	30.2(2)	33.5(1)	0(0)	38.4(2)	33(1)	0(0)	28.7(8)	27.3(8)	8(2)	18.3(2) 46.1(2)	19.7(0) 39.8(0)	21.4(0) 21.2(0)	23.1(2)	20(4)	21.7(1)
|Co|[h]	3	0	0	2	1	0	1	0	0	0	1	0	0	1	0
$\|N_p\|$[h]	2(2)	3(2)	0(0)	2(1)	6(4)	1(0)	2(2)	4(2)	5(2)	4(2)	6(5)	0(0)	3(3)	3(2)	0(0)
$\|C_a\|$[h]	2(0)	1(1)	0(0)	2(1)	3(2)	0(0)	5(3)	3(1)	2(2)	11(7)	10(9)	21(0)	4(2)	3(3)	0(0)
$\|C_b\|$[h]	1(1)	2(1)	1(0)	3(2)	5(4)	1(0)	11(3)	7(4)	4(3)	21(9)	28(10)	14(0)	6(2)	5(3)	0(0)
$\|C_m\|$[h]	1(1)	1(0)	1(0)	3(3)	6(3)	1(0)	6(4)	4(2)	5(4)	20(2)	19(4)	42(1)	6(4)	7(3)	1(1)
$\|D_{av}\|$[h]	2(1)	2(1)	1(0)	2(2)	5(3)	1(0)	6(5)	5(3)	4(3)	14(9)	16(12)	18(13)	5(3)	4(3)	0(0)
χ_{av}[i]	71(2)	77(3)	89.4(1)	73.8(3)	78.8(6)	89.6(2)	68(6)	81(4)	87(1)	67(11)	69(13)	89.9(0)	67(3)	73(4)	89.7(1)
rmsd A[j]		0.054	0.034		0.078	0.047		0.040	0.096		0.068	0.161		0.032	0.056
rmsd B[k]		0.266	0.485		0.218	0.722		0.364	0.599		0.194	0.688		0.163	0.475

[a] L^1 = 1-butylamine, L^2 = benzylamine, L^3 = phenethylamine, L^4 = 1-methylpiperazine, L^5 = piperidine, X = SbF_6, Y = NO_3. [b] Calculation on a single molecule with all nearest neighbors. [c] Gas-phase calculation. [d] Ref 18. [e] Mean axial Co−N distance (Å). [f] Mean equatorial Co−N distance (Å). [g] Mean axial ligand orientation (deg) defined as the dihedral angle between the axial ligand α-carbon and the closest porphyrin nitrogen. [h] |Co|, $|N_p|$, $|C_a|$, $|C_b|$, and $|C_m|$ are the mean absolute perpendicular displacements (in units of 0.01 Å) of the Co(III) ion, porphyrin nitrogens, α-, *β*-, and *meso*-carbons, respectively, from the 24-atom porphyrin mean plane; $|D_{av}|$ is the average for all atoms. [i] χ_{av}, mean porphyrin core−phenyl group dihedral angle (deg). [j] Root-mean-square difference (Å) for a fit of the calculated and observed structures (Co(III) ion, 24 porphyrin core atoms, and axial nitrogens). [k] Root-mean-square difference (Å) for a fit of the calculated and observed structures (all atoms).

shown in the edge-on ORTEP diagram of Figure 3, both protons of the NH_2 group of the uppermost phenethylamine ligand of **3** (i.e., that coordinated to Co via N(5) in Figure S1) are hydrogen bonded to a pair of cis fluorine atoms of the closely juxtaposed SbF_6^- anion. Similar H-bonding interactions involving one of the two NH_2 protons are observed for **1** (Figure S3).

The noncentrosymmetric crystal structure of **4** is more unusual. The axial 1-methylpiperazine ligands adopt a staggered arrangement over the porphyrin core which is clearly nonplanar. The NH proton of the uppermost ligand in Figure 1 is hydrogen bonded to a fluorine atom of the SbF_6^- anion. The distances and angle of the interaction are F(5)···H(7) = 2.258 Å, F(5)···N(7) = 3.173 Å, and F(5)···H(7)−N(7) = 167.8° (Figure 3). A solvate water molecule is hydrogen bonded to the noncoordinated nitrogen atom, N(6), of the trans 1-methylpiperazine ligand. The distance, N(6)···O(1), is 2.928 Å. The $Co-N_{ax}$ distances average to 2.040(1) Å, substantially longer than the mean $Co-N_{ax}$ distances of the bis(1° amine) complexes. The mean $Co-N_p$ distance is 1.985(13) Å. The $Co-N_{ax}$ vectors are slightly tipped relative to the heme normal; individual N_p-Co-N_{ax} angles span the range 87.5(2)−92.2(2)°. The modest off-axis tilt of the axial donor atoms is also evident from the $N_{ax}-Co-N_{ax}$ angle of 177.5(2)°. The mean $Co-N_{ax}-C_\alpha$ angle is 116.8(5)°. The axial ligand orientations, measured by the $N_p-Co-N_{ax}-C_\alpha$ dihedral angles, are 7.1(4)° (N(4)−Co−N(7)−C(61)), 43.5(5)° (N(3)−Co−N(7)−C(64)), 18.3(4)° (N(3)−Co−N(5)−C(51)), and 21.7(4)° (N(2)−Co−N(5)−C(54)). The dihedral angles between the four *meso*-phenyl groups and the 24-atom porphyrin mean plane measure 60.6(2), 82.8(2), 60.5(1), and 64.2(2)° for the phenyl rings attached to Cm(1) through Cm(4), respectively. Both the *meso*-carbons and the four pairs of *β*-carbons of the porphyrin macrocycle are alternately

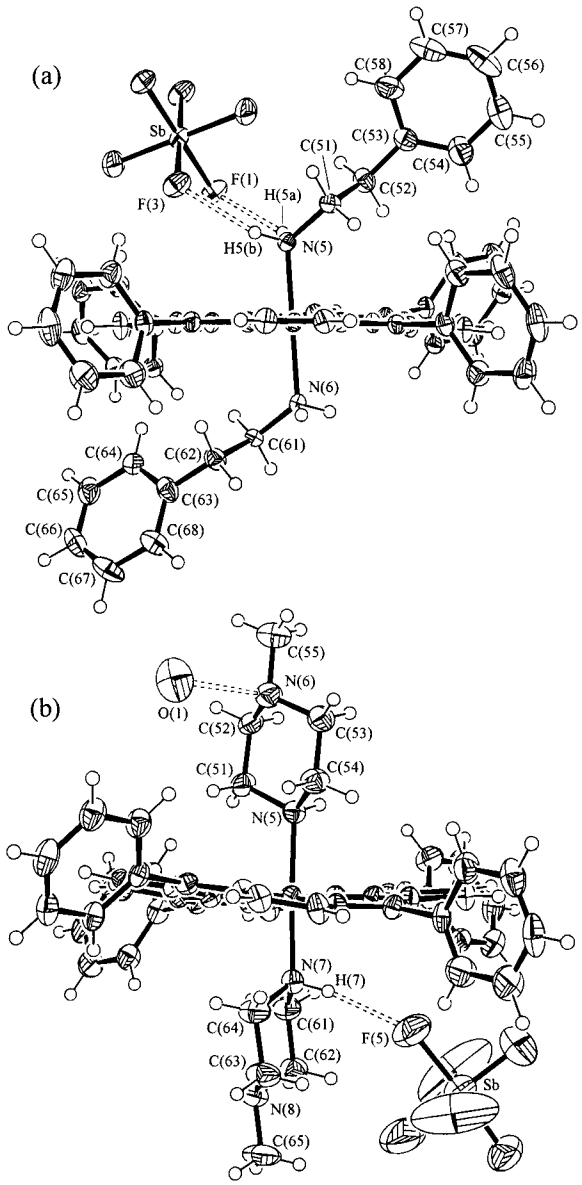

Figure 3. ORTEP diagrams (50% probability surfaces for all non-H atoms) showing the intermolecular hydrogen bonding interactions in edge-on views (parallel to the N(1)−Co−N(2) planes) of (a) $[Co(TPP)(PhCH_2CH_2NH_2)_2](SbF_6)$ and (b) $[Co(TPP)(1\text{-}MePipz)_2](SbF_6)\cdot H_2O$.

displaced above and below the porphyrin mean plane (Figure 2, Table 2).

NMR Spectroscopy. The ^1H and ^{13}C NMR spectra of **1**−**4** were consistent with the NMR spectra reported for other bis(amine) low-spin d^6 Co(III) porphyrins.[12−14] (Assigned high-resolution ^1H and ^{13}C spectra of **1** are illustrated for completeness in Figure S4.) The narrow line widths and resolved triplet patterns observed for the NH_2 protons of **1**−**3** ($^3J_{NH_2-CH_2} = 5.8-7.0$ Hz) and the NH proton of **4** ($^3J_{NH-CH_2} = 11.8$ Hz) indicate that both the spin−spin relaxation rate and the rate of axial ligand exchange are slow on the 500 MHz NMR time scale for this class of compounds.

Figure 4 shows selected ^{59}Co NMR spectra for compound **6** as a function of temperature. The ^{59}Co chemical shifts of **5**−**7**, **10**, and **11** all exhibit a linear increase (decrease in shielding) with increasing temperature (Figure 5, Table S29). The temperature coefficients (and intercepts) are 3.50(4) ppm/°C (8163(2) ppm), 3.72(2) ppm/°C (8132.6(7) ppm), 2.75(5) ppm/°C (8322(1) ppm), 3.21(6) ppm/°C (8383(2) ppm), 2.88(1) ppm/°C (8623.6(5) ppm), and 3.17(4) ppm/°C (8586(1) ppm) for [Co(TPP)Cl], **6**, **5**, **7**, **10**, and **11**, respectively. As shown in Figures 4 and 5, the ^{59}Co line widths also decrease rather markedly with increasing temperature. The narrowest lines were observed for **10** ($3.9(6)-6.5(9) \times 10^2$ Hz over the temperature range 55.1−1.4 °C). Line widths for **7** were the broadest, ranging from $3.3(0) \times 10^3$ Hz at 37.2 °C to $1.3(2) \times 10^4$ Hz at −34.5 °C. Both **8** and **9** were NMR-silent on the ^{59}Co NMR time scale, irrespective of the width of the spectral window used for data acquisition or the solution temperature. The ^1H and ^{13}C spectra of these derivatives were, however, normal. The complexes with intrinsically narrow line widths, namely **6**, **10**, and **11**, showed strong $^{59}Co-^{14}N$ spin−spin coupling between the cobalt and axially coordinated nitrogen nuclei, as evidenced by the emerging quintet pattern at higher temperatures for the ^{59}Co resonance of **6** in Figure 4. The value of $^1J_{Co-N}$ measured 600(5) Hz in each case. The sterically hindered secondary amine derivatives **10** and **11** each showed an additional signal due to the mixed-ligand intermediate, $[Co(TPP)(R_2NH)Cl]$, even with a large excess of ligand present.

Molecular Mechanics Calculations. New M−L force field parameters were developed for bis(amine) complexes of Co(III) porphyrins using the four X-ray structures of this study and that of $[Co(TPP)(Pip)_2](NO_3)$[18] for parametrization. Two types of calculation were performed for each complex: (1) a gas-phase geometry optimization on the isolated $[Co(TPP)(L)_2]^+$ cation; (2) a geometry optimization on a single $[Co(TPP)(L)_2]^+$ cation within its lattice environment. In the latter case, the lattice subset modeled comprised all neighboring cations, anions, and solvate molecules (when present). Since these calculations were computationally expensive (>5000 atoms), an initial parameter set was developed by comparison of the calculated gas phase conformations with the X-ray structures. Final adjustments to the M−L interaction parameters of the force field were made by comparing the structures calculated in the presence of all lattice neighbors with those observed crystallographically.

Metrical data comparing the calculated and X-ray coordination sphere geometries, ligand orientations, porphyrin core conformations, and *meso*-phenyl group orientations of **1**−**4** and $[Co(TPP)(Pip)_2](NO_3)$ are given in Table 2. Figure 6 depicts these data more graphically for one of the five compounds by showing least-squares fits of the MM-calculated (gas phase and solid state) and crystallographically observed structures of **4**. The results collectively demonstrate that the calculated gas phase structures fit the X-ray structures poorly on the whole. The best (rmsd = 0.034 Å) and poorest (rmsd = 0.161 Å) fits were for $[Co(TPP)(1\text{-}BuNH_2)_2]^+$ and $[Co(TPP)(1\text{-}MePipz)_2]^+$, respectively. The largest deviations between theory and experiment are for the $Co-N_{ax}$ distances, axial ligand and *meso*-phenyl group orientations, and, in the case of the nonplanar derivative **4**, the porphyrin core conformation. Significantly improved fits of the X-ray structures were obtained when a full set of nearest neighbors to the $[Co(TPP)(L)_2]^+$ cation selected for geometry optimization were included in the calculation; rmsd's ranged from 0.032 Å for $[Co(TPP)(Pip)_2](NO_3)$ to 0.078 Å for **1**.

Figure 7 compares gas phase conformational energy surfaces for $[Co(TPP)(1\text{-}BuNH_2)_2]^+$ and $[Co(TPP)(Et_2NH)_2]^+$ as plots of the change in total steric energy with axial ligand orientation. Similar plots for $[Co(TPP)(1\text{-}MePipz)_2]^+$ are given in the Supporting Information (Figure S5). The data for $[Co(TPP)(Et_2NH)_2]^+$ are included in Figure 7 even though we have not determined the X-ray structure of this complex because the conformational surface, population distribution, and energy minima are directly relevant to our interpretation of the ^{59}Co

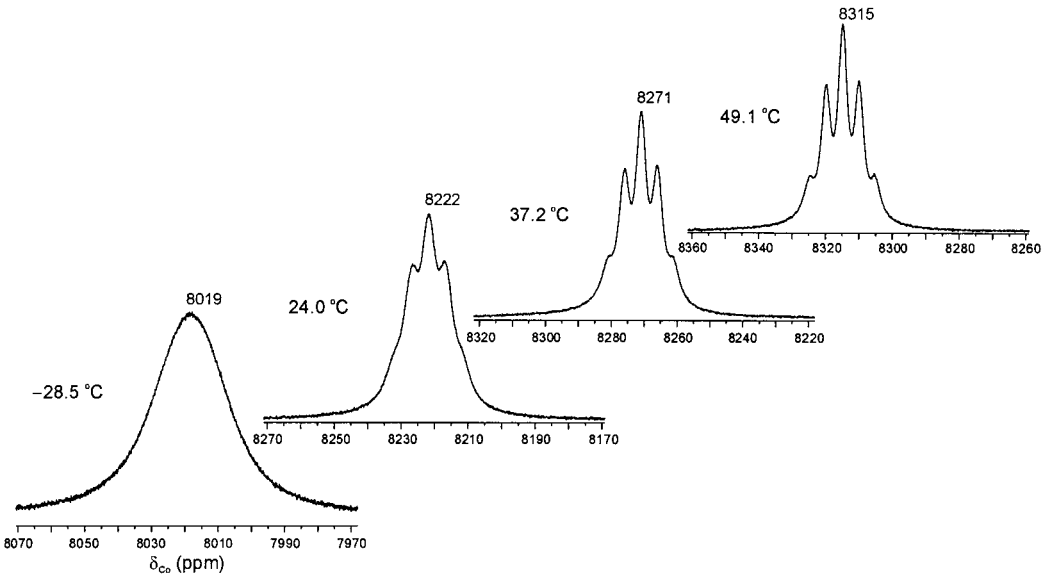

Figure 4. Selected ^{59}Co NMR spectra of [Co(TPP)($BzNH_2$)$_2$]Cl at different temperatures in 50% (v/v) ligand/$CDCl_3$ solution.

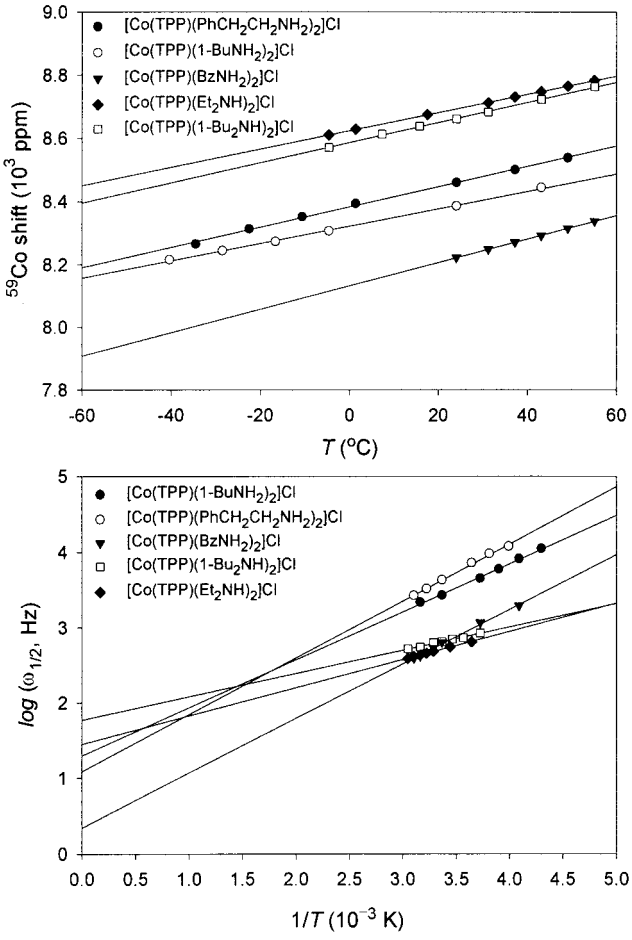

Figure 5. Plot of the variation of ^{59}Co chemical shift with temperature (top) and the log of the ^{59}Co line width, $log(\omega_{1/2})$, with reciprocal temperature (bottom) for five [Co(TPP)(amine)$_2$]Cl derivatives.

NMR spectra of [Co(TPP)(Et_2NH)$_2$]Cl and the other bis(amine) derivatives of this study.

Three types of low-energy conformation were found for [Co(TPP)(1-$BuNH_2$)$_2$]$^+$. The lowest energy conformers ($\Delta U_T = 0$ kcal/mol) have *staggered* axial ligands ($\Delta\phi = 90°$) positioned directly over a cis pair of Co−N_p bonds, e.g., ϕ_1, $\phi_2 = 0°$, 90°. The remaining two types of local minimum occur (1) when the axial ligands adopt an *anti* arrangement ($\Delta\phi = 180°$) over a trans pair of Co−N_p bonds (e.g., ϕ_1, $\phi_2 = 0°$, 180°; $\Delta U_T = 0.03$ kcal/mol) and (2) when the axial ligands are exactly *eclipsed* ($\Delta\phi = 0°$) and lie directly over a single Co−N_p bond, e.g., ϕ_1, $\phi_2 = 0°$, 0° ($\Delta U_T = 0.16$ kcal/mol). In each case, the α-CH_2 protons of the ligands are staggered relative to the pyrrole nitrogens (H···N_p ∼2.8 Å).[53]

The steric energy changes for [Co(TPP)(Et_2NH)$_2$]$^+$ are ∼7.5 times larger (ΔU_{Tmax} ∼7.5 kcal/mol) than those for [Co(TPP)-(1-$BuNH_2$)$_2$]$^+$ (Figure 7), consistent with the increased steric bulk of the axial ligands. Three types of low-energy conformations exist for the Et_2NH derivative. The N−H bonds of the axial ligands are *staggered* (90° apart) and are positioned over the bisectors of adjacent *cis*-N_p−Co−N_p angles in the lowest-energy S_4-ruffled conformations ($\Delta U_T = 0$ kcal/mol, e.g., ϕ_1, $\phi_2 = 121°$, 344°). The first type of local minimum (ΔU_T ∼3.2 kcal/mol, e.g., ϕ_1, $\phi_2 = 209°$, 344°) has a planar porphyrin core conformation and exact inversion symmetry (C_i); the N−H bonds of the axial ligands adopt an *anti* arrangement (180° apart) and lie over the bisector of a *cis*-N_p−Co−N_p angle. In the second type of local minimum (ΔU_T ∼3.3 kcal/mol, e.g., ϕ_1, $\phi_2 = 210°$, 165°) the N−H bonds of the axial ligands are *eclipsed* and lie over the bisector of a *cis*-N_p−Co−N_p angle (planar porphyrin core). For all low-energy conformations, the axial pairs of α-CH_2 protons of the ligands point toward a pair of cis porphyrin nitrogens, favoring longer nonbonded contacts (H···N_p ∼2.7 Å) than for the higher energy conformations.[54]

Molecular Dynamics Calculations. Scatter plots showing the axial ligand orientations, ϕ_1 and ϕ_2, for 6800 snapshots (0.075 ps sampling interval) taken during a typical 500 ps constant temperature (298 K) MD simulation for [Co(TPP)(1-$BuNH_2$)$_2$]$^+$ and [Co(TPP)(Et_2NH)$_2$]$^+$ are given in Figure 7. For

(52) Scheidt, W. R.; Lee, Y. J. *Struct. Bonding* **1987**, *64*, 1−70.

(53) Three unique types of high-energy conformation (energy differences > 0.02 kcal/mol) exist for [Co(TPP)(1-$BuNH_2$)$_2$]$^+$: (1) conformations with *staggered* axial ligands (relative orientations, $\Delta\phi$, of 90°) positioned approximately over adjacent porphyrin *meso*-carbons, e.g., ϕ_1, $\phi_2 = 45°$, 225° ($\Delta U_T = 0.96$ kcal/mol), (2) conformations with an *anti* axial ligand arrangement ($\Delta\phi = 180°$) over the bisector of a *cis*-N_p−Co−N_p angle, e.g., ϕ_1, $\phi_2 = 45°$, 135° ($\Delta U_T = 1.05$ kcal/mol), and (3) conformations with an *eclipsed* axial ligand arrangement ($\Delta\phi = 0°$) over the bisector of a *cis*-N_p−Co−N_p angle, e.g., ϕ_1, $\phi_2 = 45°$, 315° ($\Delta U_T = 1.23$ kcal/mol). In each case, the α-CH_2 protons of the butylamine ligands point at adjacent pyrrole nitrogens (H···N_p ∼2.6 Å).

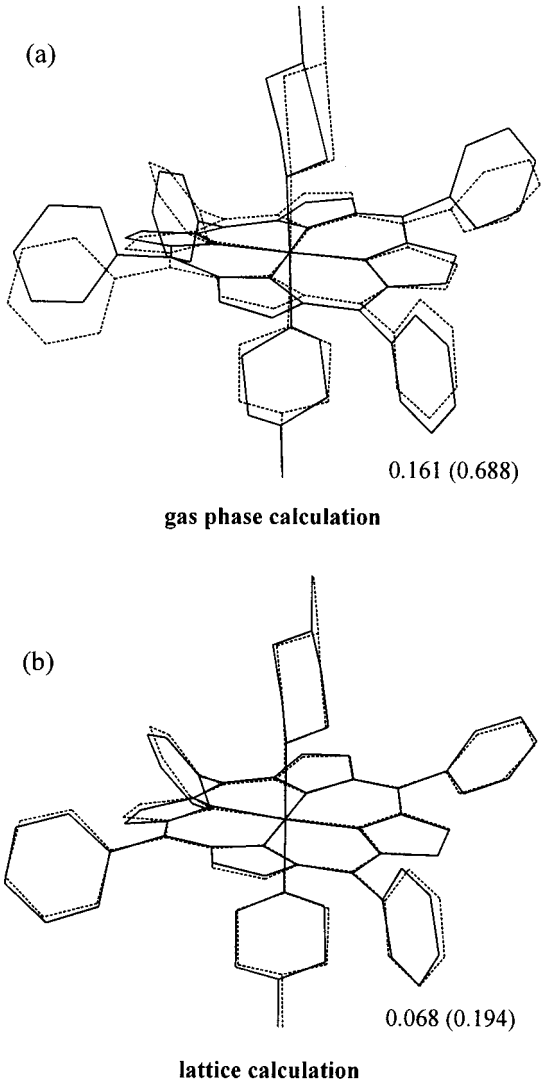

Figure 6. Comparison of MM-calculated (solid lines) and crystallographically observed (broken lines) structures of $[Co(TPP)(1\text{-}MePipz)_2](SbF_6)\cdot H_2O$. The gas-phase MM-calculated structure is shown in (a); the structure calculated in the presence of all lattice neighbors is shown in (b). Two rmsd's (in Å) are shown for each fit. The first is for the Co(III) ion, the 24 porphyrin core atoms, and the two axial nitrogens. The second (in parentheses) is for all non-hydrogen atoms. Hydrogen atoms have been omitted for clarity.

$[Co(TPP)(1\text{-}BuNH_2)_2]^+$, all minima on the potential energy surface have a high population frequency. However, the global minima (e.g., ϕ_1, ϕ_2 = 90°, 90°) show a slightly higher population density than the local minima (e.g., ϕ_1, ϕ_2 = 90°, 180°). The pathway from one minimum to the next occurs mainly through the saddle points on the surface, as evidenced by the relatively high population densities linking the minima (e.g., ϕ_1, ϕ_2 = 90°, 135°). High energy conformations of $[Co(TPP)(1\text{-}BuNH_2)_2]^+$ (e.g., ϕ_1, ϕ_2 = 45°, 225°) are only occasionally populated. In marked contrast, only one of several possible low-energy S_4-ruffled conformations of $[Co(TPP)(Et_2NH)_2]^+$ is significantly populated (ϕ_1, ϕ_2 = 121, 344°) throughout the MD simulation period. The adjacent local minimum with C_i symmetry (ϕ_1, ϕ_2 = 209, 344°) and a planar porphyrin core geometry is also partially populated at 298 K during the simulation. From Figure 7, high-energy conformations of $[Co(TPP)(Et_2NH)_2]^+$ are clearly not populated during the 500-ps interval. A similar MD trajectory was obtained for the related bis(secondary amine) derivative $[Co(TPP)(1\text{-}MePipz)_2]^+$ (Figure S5).

DFT Calculations. Valence orbital (4s, 4p, and 3d) electron populations computed at the B3LYP/LACVP level of theory are given in Table 3 along with values of the electric field gradient, q_{val}, calculated from the Townes−Dailey approximation (eq 3),[55−57]

$$q_{val} = \frac{4}{5}\langle r^{-3}\rangle_{4p}\left\{-N_{p_z} + \frac{1}{2}(N_{p_x} + N_{p_y})\right\} + \frac{4}{7}\langle r^{-3}\rangle_{3d}\left\{N_{dx^2-y^2} - N_{d_{z^2}} + N_{d_{xy}} - \frac{1}{2}(N_{d_{xz}} + N_{d_{yz}})\right\} \quad (3)$$

where N_p and N_d are the calculated electron populations of the individual 4p and 3d orbitals. $\langle r^{-3}\rangle_{3d}$ and $\langle r^{-3}\rangle_{4p}$ are the expectation values of $1/r^3$ taken over the 3d and 4p radial functions, respectively. The value of $\langle r^{-3}\rangle_{3d}$ was determined for each complex from the total 3d electron population by interpolation between the following estimated expectation values: 5.36 au for Co configuration $3d^7$, 6.08 au for $3d^6$, and 6.84 au for $3d^5$. These estimates are based on those reported by Weissbluth and Maling[58] for iron, but are corrected for the well-known variation of $\langle r\rangle$ with atomic number.[59,60] The value of $\langle r^{-3}\rangle_{4p}$ was taken as $1/3\langle r^{-3}\rangle_{3d}$.[61]

The total 3d electron population varies from 7.6189 for the C_i symmetry conformation of $[Co(TPP)(Et_2NH)_2]^+$ to 7.6731 for [Co(TPP)Cl]. The electron populations of individual 3d orbitals vary considerably with the nature of the axial ligand and the porphyrin core conformation; the $3d_{z^2}$ orbital shows the largest population variation from 0.3853 in [Co(TPP)Cl] to 1.6820 in $[Co(TPP)(1\text{-}BuNH_2)_2]^+$. A significant increase in the $3_{d_{yz}}$ population from 0.9377 in $[Co(TPP)(1\text{-}BuNH_2)_2]^+$ to 1.9821 in the C_i symmetry conformation of $[Co(TPP)(Et_2NH)_2]^+$ is also evident. The 4p electron populations are similar for the $[Co(TPP)(L)_2]^+$ derivatives listed in Table 3 and show very minor changes with axial ligand orientation in the case of $[Co(TPP)(Et_2NH)_2]^+$. The electric field gradient, q_{val}, is smallest for the C_i symmetry conformation of $[Co(TPP)(Et_2NH)_2]^+$ (0.0209) and largest for $[Co(TPP)(PhCH_2CH_2NH_2)_2]^+$ (0.1060). The sign of q_{val} is negative for the S_4-ruffled conformations of $[Co(TPP)(Et_2NH)_2]^+$ and $[Co(TPP)(1\text{-}Bu_2NH)_2]^+$ and the local minimum conformation of $[Co(TPP)(Et_2NH)_2]^+$ in which the axial ligand N−H groups are eclipsed and oriented over a C_m−Co vector (C_s symmetry). The natural atomic charges of the Co(III) ion vary from +1.0014 in $[Co(TPP)(BzNH_2)_2]^+$ to +1.0823 in the

(54) As with $[Co(TPP)(1\text{-}BuNH_2)_2]^+$, three types of high-energy conformations exist for $[Co(TPP)(Et_2NH)_2]^+$. In the highest energy conformations (ΔU_T ~7.5 kcal/mol, e.g., ϕ_1, ϕ_2 = 85°, 100°), the N−H bonds of the axial ligands adopt an *anti* arrangement (180° apart over a planar porphyrin core) and lie approximately over a pair of *trans*-Co−N_p bonds (within 15°). The next highest energy maxima (ΔU_T ~5.8 kcal/mol) are slightly S_4-ruffled and occur when the N−H bonds of the axial ligands are *eclipsed* (< 20° apart) and lie over a single Co−N_p bond, e.g., ϕ_1, ϕ_2 = 177°, 200°. The least strained high-energy structures have slightly saddled porphyrin cores and arise when the axial ligand N−H bonds are *staggered* (~60° apart) and lie within 20° of an orthogonal pair of Co−N_p bonds (ΔU_T ~5.4 kcal/mol, e.g., ϕ_1, ϕ_2 = 177°, 122°). In each case, the α-CH_2 groups of the ligands come close to eclipsing a pair of trans porphyrin nitrogens, leading to short nonbonded contacts (H···N_p ~2.4 Å) and a high steric energy.

(55) Townes, C. H.; Dailey, B. P. *J. Chem. Phys.* **1949**, *17*, 782−796.
(56) Bancroft, G. M.; Mays, M. J.; Prater, B. E. *J. Chem. Soc. A* **1970**, 956−968.
(57) Grodzicki, M.; Männing, V.; Trautwein, A. X.; Friedt, J. M. *J. Phys. B: At. Mol. Phys.* **1987**, *20*, 5595−5625.
(58) Weissbluth, M.; Maling, J. E. *J. Chem. Phys.* **1967**, *47*, 4166−4172.
(59) Cowan, R. D. *The Theory of Atomic Structure and Spectra*; University of California Press: Berkley, 1981; p 236.
(60) Mason, J. *Chem. Rev.* **1987**, *87*, 1299−1312.
(61) Trautwein, A. *Struct. Bonding* **1974**, *20*, 101−167.

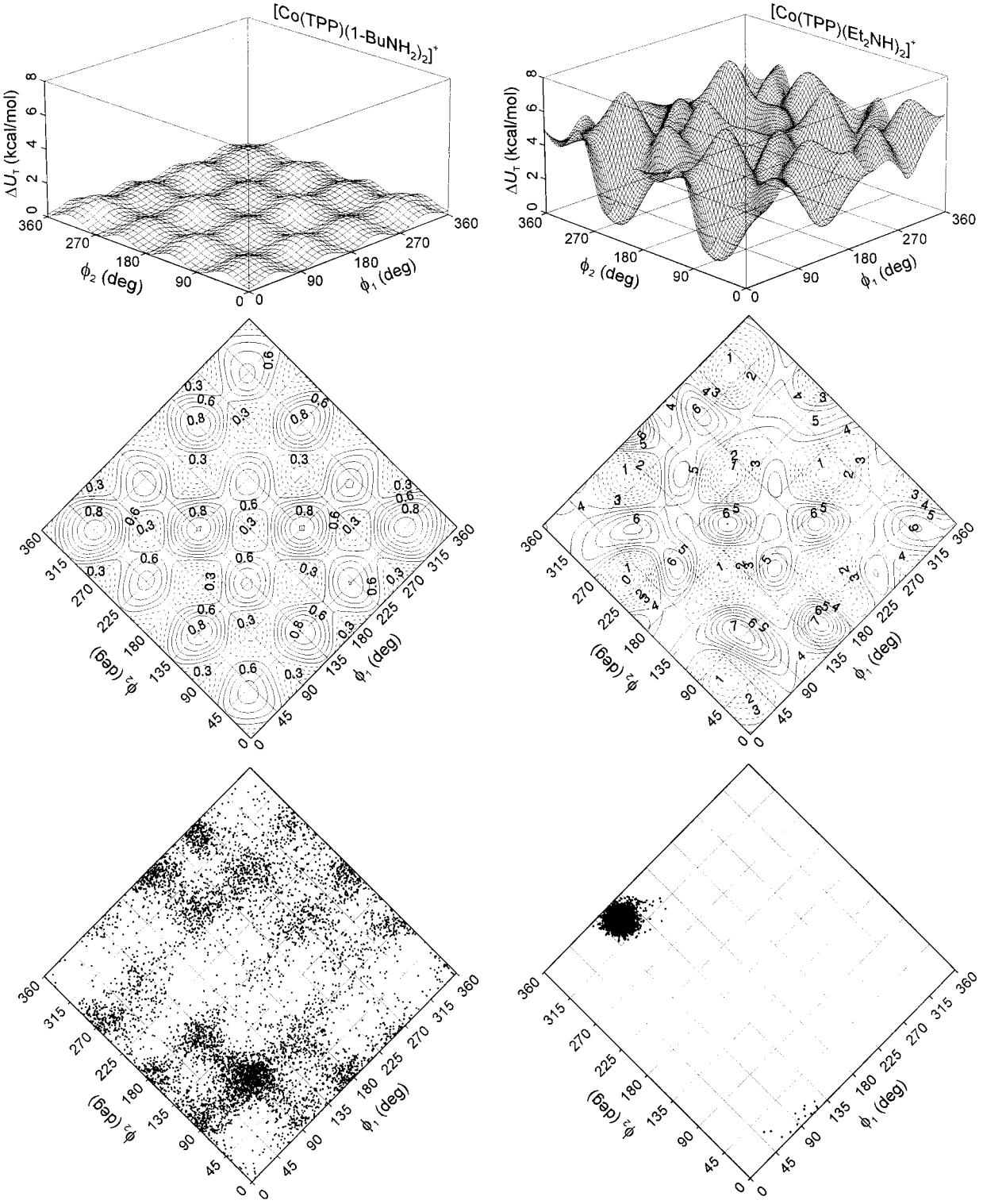

Figure 7. Surface plot of the change in steric energy (ΔU_T) as a function of axial amine orientation for $[Co(TPP)(1\text{-}BuNH_2)_2]^+$ and $[Co(TPP)(Et_2NH)_2]^+$ (top). The center plots are contour maps of the three-dimensional surfaces; broken lines indicate regions encompassing minima on each surface. The bottom graphs are scatter plots showing 6800 out of a total of 68 000 sampled conformations during a 500 ps MD simulation for each complex at 298 K in the gas phase. In each plot, ϕ_1 and ϕ_2 correspond to the dihedral angles $N_p-Co(III)-N_{ax}-C_\alpha$ for the top and bottom ligands, respectively.

C_s symmetry conformation of $[Co(TPP)(Et_2NH)_2]^+$. The primary amine complexes exhibit higher axial nitrogen charge densities (ranging from −0.7806 in the 1-$BuNH_2$ derivative to −0.7870 in the $PhCH_2CH_2NH_2$ derivative) than the secondary amine complexes where $q_{N_{ax}}$ varies from −0.6025 in $[Co(TPP)(1\text{-}Bu_2NH)_2]^+$ to −0.6080 in the C_s symmetry conformation of $[Co(TPP)(Et_2NH)_2]^+$.

Discussion

Molecular and Crystal Structures. The X-ray structures of **1**−**3** are the first examples of α-unsubstituted primary amine complexes of Co(III) porphyrins. They are also isoelectronic, but not isomorphous, with the structurally analogous Fe(II) complexes;[9] each has an essentially planar porphyrin core

Table 3. DFT-Calculated d-Orbital Electron Populations and Selected Mean Atomic Charges for $[Co(TPP)(L)_2]^+$ Complexes[a,b]

	1-$BuNH_2$	$BzNH_2$	$PhCH_2CH_2NH_2$	Et_2NH[c]	Et_2NH[d]	Et_2NH[e]	1-Bu_2NH[c]	[Co(TPP)Cl][f]
4s	0.0035	0.0038	0.0036	0.0039	0.2592	0.2589	0.2538	0.2826
$4p_x$	0.0008	0.0011	0.0010	0.0013	0.0011	0.0011	0.0016	0.0036
$4p_y$	0.0012	0.0012	0.0010	0.0017	0.0015	0.0015	0.0015	0.0036
$4p_z$	0.0012	0.0012	0.0011	0.0013	0.0012	0.0011	0.0016	0.0027
$3d_{x^2-y^2}$	1.3624	1.1965	1.7841	0.9132	0.9176	0.9035	0.9512	1.5483
$3d_{z^2}$	1.6820	1.5817	1.5894	1.0844	1.0632	1.0658	1.1360	0.3853
$3d_{yz}$	0.9377	1.0662	1.5442	1.9758	1.9821	1.9790	1.9470	1.9639
$3d_{xz}$	1.9073	1.9312	1.4220	1.6922	1.6868	1.6927	1.6477	1.9639
$3d_{xy}$	1.7723	1.8933	1.3266	1.9781	1.9785	1.9779	1.9650	1.8117
Total (3d)	7.6617	7.6689	7.6663	7.6437	7.6372	7.6189	7.6469	7.6731
$\langle r^{-3}\rangle_{3d}$	4.8636	4.8583	4.8602	4.8770	4.8818	4.8953	4.8746	4.8552
Total (val)	7.6653	7.6706	7.6698	7.6475	7.8964	7.8777	7.9006	7.9556
EFG, q_{val}	0.0837	0.0260	0.1060	−0.0753	0.0209	−0.0564	−0.0478	2.8055
q_{Co}	1.0093	1.0014	1.0091	1.0561	1.0635	1.0823	1.0547	1.0222
q_{N_p}	−0.5309(11)	−0.5308(61)	−0.5304(26)	−0.5327(71)	−0.498(29)	−0.537(11)	−0.5329(79)	−0.4984(0)
$q_{N_{ax}}$	−0.7806(1)	−0.7769(0)	−0.7870(2)	−0.6054(5)	−0.6067(0)	−0.6080(1)	−0.6025(41)	−0.6152(0)[g]

[a] All geometries, except that of [Co(TPP)Cl], were energy minima derived from MM calculations. DFT calculations were single point calculations on the $S = 1$ ground-state configurations with the LACVP basis set (B3LYP method). [b] Populations and charges in electronic charge units. [c] S_4-ruf[52] porphyrin core conformation. [d] C_i-symmetry local minimum ($\Delta U_T = 3.149$ kcal/mol; $\phi_1 = 70°$, $\phi_2 = 20°$). [e] Local minimum ($\Delta U_T = 3.864$ kcal/mol; $\phi_1 = 70°$, $\phi_2 = 290°$). [f] DFT-optimized geometry (C_4 symmetry). [g] Charge on axial chloride ligand.

conformation. The X-ray structure of **4**, although not the only structure of a bis(secondary amine) Co(III) porphyrin,[2,18] is nonetheless remarkable because hydrogen bonding interactions within the lattice which involve the axial piperazine ligands render the structure noncentrosymmetric. Moreover, the partly staggered relative orientations of the axial ligands lead to a significantly nonplanar conformation for the tetrapyrrole ligand (*vide infra*), a phenomenon more commonly observed with sterically hindered porphyrin ligands.[2,3,38,62,63]

The $Co-N_{ax}$ bonds of **1**−**3** average 1.980(5) Å and compare favorably with the axial bond distance reported for [Co(TPP)-$(PhCH(CH_3)NH_2)_2$]Br (1.983 Å),[19] even though the axial ligands in the latter complex are substituted at the α-carbon. The $Co-N_{ax}$ distances of the α-unsubstituted primary amines of this study are also equivalent (within 4σ) to those reported for [Co(TMCP)-$((S)$-2-butylamine$)_2]^+$ (1.985(10) and 2.023(10) Å).[3] This is somewhat unexpected since the chiral porphyrin ligand in the latter complex is strongly S_4-ruffled and provides an orthogonal pair of ligand binding cavities above and below the porphyrin ring. The rather similar $Co-N_{ax}$ distances of the available crystallographically characterized bis(1° amine) Co(III) porphyrins suggest that primary amines bind in a sterically efficient manner. This conclusion is verified by the conformational energy surface for $[Co(TPP)(1\text{-}BuNH_2)_2]^+$ (Figure 7) which shows that the coordination of primary amines by sterically unhindered Co(III) porphyrins is characterized by steric strain energies < 1.2 kcal/mol.

The mean $Co-N_{ax}$ distance of **4** (2.040(2)°) is significantly longer than that observed for the bis(1° amine) derivatives, consistent with a larger steric bulk for the secondary amine ligands and an attendant increase in van der Waals repulsion between the porphyrin core atoms and the axial ligand α-CH_2 hydrogens. Interestingly, the $Co-N_{ax}$ distances for the 1-MePipz derivative are somewhat shorter than those reported for [Co-$(TPP)(Pip)_2](NO_3)$ (2.060(3) Å), although they may be regarded as being equivalent within 4σ. The main difference in the structures of these two secondary amine derivatives is that the porphyrin core conformation of **4** is a mixture of two types of distortion (S_4-ruf and D_{2d}-sad),[52,64] whereas the porphyrin core of $[Co(TPP)(Pip)_2](NO_3)$ is effectively planar (C_i symmetry). The S_4-ruf perturbation in **4** clearly favors a sterically efficient approach of the axial ligands and thus shorter $Co-N_{ax}$ distances. The modest distortion from planarity in the bis(1-MePipz) complex is brought about by a noncentrosymmetric arrangement of the axial ligands above and below the porphyrin core (Figures 1−3) and significant tilting (by up to 30° from the heme normal) of the *meso*-phenyl groups.[65] The unusual axial ligand arrangement primarily reflects the H-bonding interactions within the lattice while the canted *meso*-phenyl substituents are consistent with crystal packing interactions, a well documented[9,52,66] phenomenon that is clearly demonstrated by the MM-calculated conformations of Figure 6 and Table 2.

The mean $Co-N_p$ distances of compounds **1** (1.987(11) Å), **2** (1.987(4) Å), **3** (1.986(3) Å), and **4** (1.985(13) Å) are equivalent and compare favorably with the mean $Co-N_p$ distance of 1.985(3) Å reported for $[Co(TPP)(PhCH(CH_3)NH_2)_2]$-Br.[19] The sizable dispersion in the $Co-N_p$ distances of the $BzNH_2$ and 1-MePipz derivatives indicates that the equatorial coordination group distances are asymmetric; the shorter $Co-N_p$ distances are to the porphinato nitrogens that are within 40° of the planes containing the ligand α-carbons (Table 1). We attribute most, but not all, of the in-plane asymmetry of the $Co-N_p$ bonds to crystal packing effects because the MM-calculated structures only begin to reproduce (∼50−60%) the dispersion in the $Co-N_p$ bond distances when carried out in the presence of all lattice neighbors (Table 2).

Finally, the axial ligand orientations (measured by the $N_p-Co-N_{ax}-C_\alpha$ dihedral angles) vary markedly from 0° for the

(62) Munro, O. Q.; Serth-Guzzo, J. A.; Turowska-Tyrk, I.; Mohanrao, K.; Shokhireva, T. Kh.; Walker, F. A.; Debrunner, P. G.; Scheidt, W. R. *J. Am. Chem. Soc.* **1999**, *121*, 11144−11155.

(63) Senge, M. O. In *The Porphyrin Handbook*; Kadish, K. M., Smith, K. M., Guilard, R., Eds.; Academic: New York, 2000; Vol. 1, pp 239−347.

(64) Shelnutt, J. A. In *The Porphyrin Handbook*; Kadish, K. M., Smith, K. M., Guilard, R., Eds.; Academic: New York, 2000; Vol. 7, pp 167−223.

(65) Although nonplanar, the structure of **4** is considerably less distorted than that of $[Co(TMCP)((S)$-2-butylamine$)_2]^+$.[3] The mean absolute perpendicular displacement of the *meso*-carbons of the chiroporphyrin derivative measures 0.63(4) Å;[3] the equivalent parameter for **4** is only ∼30% of this value (0.20(2) Å). The large S_4-ruf distortion for [Co-$(TMCP)((S)$-2-butylamine$)_2]^+$ results from the presence of four sterically bulky α,*β*,α,*β*-*meso*-cyclopropyl substituents rather than the steric bulk of the axial ligands, as is the case for **4**. The marked S_4-ruffling of the chiroporphyrin macrocycle also leads to compression of the $Co-N_p$ bonds to a rather short mean distance of 1.949(11) Å.

(66) Scheidt, W. R. In *The Porphyrin Handbook*; Kadish, K. M., Smith, K. M., Guilard, R., Eds.; Academic: New York, 2000; Vol. 3, pp 49−112.

four X-ray structures (Table 2). The conformation observed in each crystal structure is therefore significantly different from a local or global minimum on the conformational energy surface for the molecule in the gas phase (Figure 7). The dominant role of intermolecular interactions in controlling the conformations of simple bis(amine) Co(III) porphyrins reflects two main factors. (1) π-Bonding between the axial ligands and the d_π orbitals is not possible for alkylamines since π-symmetry MOs with nonvanishing amplitude on the N-donor atom are absent. (2) The steric energy penalties to rotation of the axial ligands, particularly in the bis(1° amine) derivatives, are relatively small.

^{59}Co Chemical Shifts. The ^{59}Co chemical shifts of [Co(TPP)Cl], **5**−**7**, **10**, and **11** all increase linearly with increasing temperature (Figure 5 and Table S29). The extent of nuclear shielding in diamagnetic Co(III) complexes and its temperature dependence is usually interpreted with Ramsey's magnetic shielding theory (vide infra).[67] The nuclear screening constant, σ_{Co}, in the Larmor frequency equation (eq 4)

$$\nu_{Co} = \frac{\gamma_{Co}}{2\pi} B_0(1 - \sigma_{Co}) \tag{4}$$

where ν_{Co}, γ_{Co}, and B_0 are the Larmor frequency, the magnetogyric ratio, and the applied magnetic field, respectively, is given by

$$\sigma_{Co} = A - B/\Delta E \tag{5}$$

The two terms A and $B/\Delta E$ in eq 5 correspond to the diamagnetic (σ^d) and paramagnetic (σ^p) contributions to the shielding, respectively (i.e., $\sigma_{Co} = \sigma^d + \sigma^p$). Because the magnitude of A is determined by the core electrons of the nucleus in question,[68,69] it is independent of both the ligand field environment and the temperature of the system for a constant spin and oxidation state. The magnitude of the paramagnetic term $B/\Delta E$ is, however, governed by the symmetry and nature of the coordination sphere of the metal ion. For simple O_h Co(III) coordination complexes, ΔE is the energy difference between the $^1A_{1g}$ (ground) and $^1T_{1g}$ terms for the low-spin d^6 ion. A linear relationship is observed between the ^{59}Co chemical shift and the wavelength of the $^1A_{1g} \rightarrow {}^1T_{1g}$ transition in complexes with unobscured d−d transitions.[70] For a complex with effective C_{2v} symmetry (the Co(III) derivatives of this study have nondegenerate porphyrin and metal π-symmetry orbitals, consistent with < 4-fold symmetry), the $^1T_{1g}$ term will be split into its subterms $^1A_2$, $^1B_1$, and $^1B_2$. The paramagnetic term of eq 5 is thus inversely proportional to the mean energy of the $^1A_1 \rightarrow {}^1A_2$, $^1A_1 \rightarrow {}^1B_1$, and $^1A_1 \rightarrow {}^1B_2$ transitions, eq 6,

$$\sigma^p(C_{2v}) = \frac{-8\mu_0\mu_B^2}{\pi}\langle r^{-3}\rangle_{3d} \times \left[\frac{\eta(^1A_2)}{3\Delta E(^1A_2)} + \frac{\eta(^1B_1)}{3\Delta E(^1B_1)} + \frac{\eta(^1B_2)}{3\Delta E(^1B_2)}\right] \tag{6}$$

where μ_0, μ_B, and $\langle r^{-3}\rangle_{3d}$ are the vacuum permeability, the Bohr magneton, and the expectation value of $1/r^3$ taken over the 3d radial function for the Co^{3+} ion, respectively. The parameters

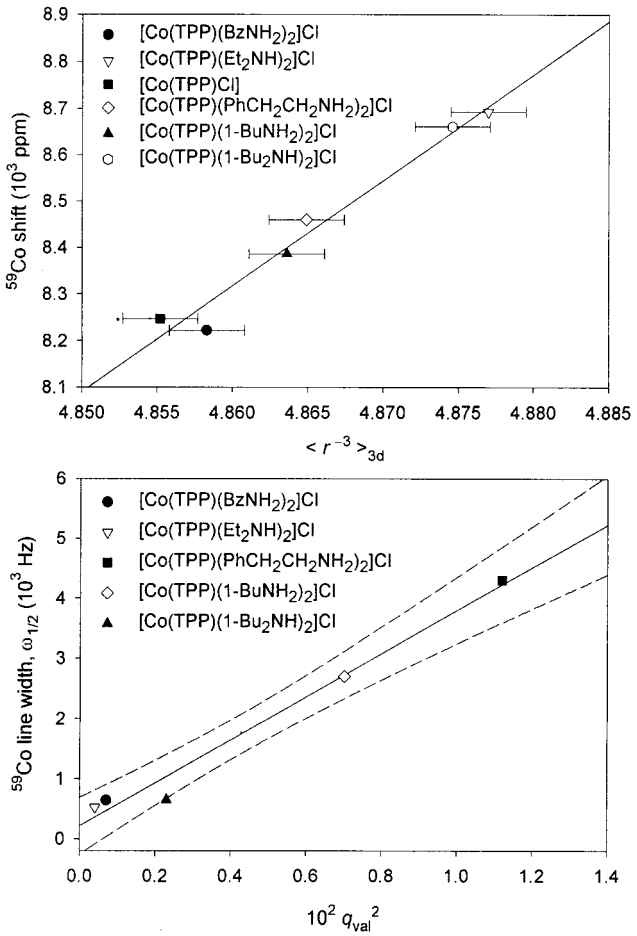

Figure 8. Plot of the relationship between the ^{59}Co chemical shift and the radial expectation value $\langle r^{-3}\rangle_{3d}$ for the Co(III) ion (top) and the dependence of the ^{59}Co line width, $\omega_{1/2}$, on the square of the electric field gradient, q_{val}^2, (bottom) for several low-spin Co(III) porphyrins. The 95% confidence interval is shown in the lower plot.

$\eta(^1A_2)$, $\eta(^1B_1)$, and $\eta(^1B_2)$ are covalency (nephelauxetic) parameters for the three excited-state terms.[70−72] The decrease in shielding with increasing temperature for [Co(TPP)Cl] and the five bis(amine) complexes of Figure 5 therefore reflects an increase in the population of the higher-lying vibrational levels of the $^1A_1$ ground state. This lowers the $^1A_1 \rightarrow {}^1A_2$, $^1A_1 \rightarrow {}^1B_1$, and $^1A_1 \rightarrow {}^1B_2$ transition frequencies and *increases* the contribution (deshielding) of the paramagnetic term in eq 6 to the shielding of the Co(III) nucleus.

A second, often overlooked factor is the variable nature of $\langle r^{-3}\rangle_{3d}$ for the complex.[70] Specifically, as the mean Co−N distance increases with the heightened vibrational amplitude of the M−L bonds at higher temperatures, a decrease in the total 3d electron population from poorer σ-donation is to be expected. Depopulation of the 3d orbitals, even if slight, will lead to an increase in the magnitude of $\langle r^{-3}\rangle_{3d}$ and thus the relative importance of σ^p to the nuclear shielding. As shown in Figure 8, a good linear correlation between the ^{59}Co shift and $\langle r^{-3}\rangle_{3d}$ exists, confirming the relationship of eq 6. Interestingly, the calculated values of $\langle r^{-3}\rangle_{3d}$ appear to be sensitive to the conformation of the complex. This is illustrated for **10** in Table 3. The S_4-ruf conformation ($Co-N_p = 1.969(3)$ Å, $Co-N_{ax} = 2.057(0)$ Å, Figure S6) has a smaller value of $\langle r^{-3}\rangle_{3d}$ than the

(67) Ramsey, N. F. *Phys. Rev.* **1950**, *78*, 699−703.
(68) Freeman, R.; Murray, G. R.; Richards, R. E. *Proc. R. Soc. London* **1957**, *A242*, 455−466.
(69) Kidd, R. G.; Goodfellow, R. J. In *NMR and the Periodic Table*; Harris, R. K., Mann, B. E., Eds.; Academic: New York, 1978; pp. 195−278.
(70) Juranić, N. *J. Chem. Phys.* **1981**, *74*, 3690−3693.
(71) Juranić, N. *Inorg. Chem.* **1980**, *19*, 1093−1095.
(72) Eichele, K.; Chan, J. C. C.; Wasylishen, R. E.; Britten, J. F. *J. Phys. Chem. A* **1997**, *101*, 5423−5430.

C_i symmetry planar conformation (Co−N_p = 1.989(2) Å, Co−N_{ax} = 2.078(0) Å), consistent with somewhat shorter M−L distances and a commensurate increase in total 3d electron density due to better σ donation. The conformation dependent spread in $\langle r^{-3}\rangle_{3d}$ values for each derivative in Table 3 and Figure 8 is estimated to be about 0.0025 au. It follows that a large change in $\langle r^{-3}\rangle_{3d}$ (of the order of 0.005−0.010 au) is required before a statistically significant difference in the ^{59}Co chemical shift can be predicted from the calculated $\langle r^{-3}\rangle_{3d}$ values for this class of Co(III) complexes. Several other important factors may also contribute to the magnitude of the ^{59}Co chemical shift observed for a particular complex. These include variations in the mean energy of the $^1A_1 \rightarrow {}^1A_2$, $^1A_1 \rightarrow {}^1B_1$, and $^1A_1 \rightarrow {}^1B_2$ transitions for the different Co(III) derivatives as well as variations in the solvent dielectric constant, particularly since 50% (v/v) amine/$CDCl_3$ solutions were used to acquire the ^{59}Co NMR spectra of each derivative. Significant solvent and counterion effects on ^{59}Co chemical shifts have in fact been reported by Edwards and co-workers[20−22] for bis(imidazole) complexes of Co(III) *meso*-tetraarylporphyrins.

A significant outcome of the relationship between the ^{59}Co chemical shifts and the total 3d electron population, or $\langle r^{-3}\rangle_{3d}$, is that a quantitative measure of the σ-donor strengths of the axial ligands is immediately apparent. From Figure 8, the σ-donor power of the ligands in this series of $[Co(TPP)(L)_2]^+$ derivatives follows the following order: $BzNH_2 \geq Cl^- > 1\text{-}BuNH_2 > PhCH_2CH_2NH_2 > 1\text{-}Bu_2NH > Et_2NH$. Importantly, this order *cannot* be predicted from the pK_as of the ligands[73] or the Mulliken populations of the free ligand donor atoms. Since the d−d absorption bands of the low-spin d^6 ion are completely obscured by bands from the strongly allowed porphyrin $\pi \rightarrow \pi^*$ transitions, electronic spectroscopy cannot be used to gauge the ligand field strength at the metal either. Thus, when combined with an accurate calculation of the total 3d electron population for the metal, ^{59}Co NMR spectroscopy is the only reliable method for measuring the axial ligand field strength in Co(III) porphyrins.

^{59}Co Line Widths and Electric Field Gradients. In addition to changes in nuclear shielding, there are marked changes in the ^{59}Co line widths with temperature. Figure 5 shows that the line widths decrease linearly with increasing temperature. For a single quadrupolar nucleus of spin I, for which quadrupole relaxation is the dominant spin relaxation mechanism, and for which molecular motion is characterized by an isotropic tumbling correlation time τ_c, the line width is given by eq 7,

$$\omega_{1/2} = \frac{3\pi}{10}\frac{(2I+3)}{I^2(2I-1)}\chi^2\left(1+\frac{1}{3}\eta^2\right)\tau_c \qquad (7)$$

where χ and η are the nuclear quadrupole coupling constant and asymmetry parameter, respectively.[69] The nuclear quadrupole coupling constant is given by eq 8,

$$\chi = \frac{e^2 q_{zz} Q}{h} \qquad (8)$$

where e is the charge on the electron, q_{zz} the principal component of the EFG at the nucleus, and Q the nuclear electric quadrupole moment.[69] The asymmetry parameter lies in the range $0 < \eta < 1$ and is given as $\eta = (q_{yy} - q_{xx})/q_{zz}$. The rotational correlation time, τ_c, is temperature-dependent (eq 9),[77]

$$\tau_c = \tau_c^0 \exp\left(\frac{V_c}{RT}\right) \qquad (9)$$

and proportional to the hydrodynamic volume, a^3, of the solute and the viscosity, ζ, of the solvent:[78,79]

$$\tau_c = (4\pi/3)(a^3\zeta/kT) \qquad (10)$$

The activation energy for tumbling, V_c, is therefore dependent on both a and ζ. Importantly, a plot of the log of the line width against reciprocal temperature may be used to determine the activation energy V_c for a range of related Co(III) complexes (eq 11):[77]

$$\log(\omega_{1/2}) = \log A + \frac{V_c}{R}\left(\frac{1}{T}\right) \qquad (11)$$

Equation 11 therefore permits straightforward quantification of the effect that the reduction in solvent viscosity with increasing temperature has on the tumbling rate and rotational correlation time through the variation in line width. From the fitted data in Figure 5, the following activation energies (and intercepts) were obtained for the six Co(III) complexes: **11**, 2.6(1) kJ mol^{-1} (1.77(5)); **10**, 3.12(6) kJ mol^{-1} (1.45(2)); [Co(TPP)Cl], 3.8(2) kJ mol^{-1} (2.08(7)); **5**, 5.3(2) kJ mol^{-1} (1.29(7)); **6**, 6.0(2) kJ mol^{-1} (0.34(7)); and **7**, 6.3(2) kJ mol^{-1} (1.09(8)). Interestingly, there is no obvious correlation between the measured values of V_c and the calculated[35] van der Waals volumes of the molecules, as might have been expected from eq 10. However, the viscosities of the $CDCl_3$/amine mixtures used for acquisition of the ^{59}Co NMR spectra are probably not constant across the series and this is likely to have contributed in part to the observed order of V_c values. Perhaps more interesting from a structural standpoint is the fact that the nonplanar complexes **11** (S_4-ruf), **10** (S_4-ruf), and [Co(TPP)Cl] (C_{4v} dome) all have relatively small activation energies for molecular reorientation, while those that are conformationally flexible exhibit significantly higher activation energies. The marked difference in conformational flexibility between $[Co(TPP)(1\text{-}BuNH_2)_2]^+$ and $[Co(TPP)(Et_2NH)_2]^+$ is strikingly demonstrated in the plots of the MD trajectories of these two systems at 298 K in Figure 7. Provided that the solvent viscosities and hydrodynamic radii of the species being compared are reasonably similar, it is not untenable to suggest from the gas phase MD data in Figure 7 that a spread in conformational isomers in solution may lead to a mean activation energy barrier for molecular reorientation that is overall higher than that for a system which largely populates a single type of conformation in solution.

For a constant temperature, e.g., 24 °C, the NMR data in Figure 5 and Table S29 show that the ^{59}Co line widths follow the order **10** < **6** < **11** < **5** < [Co(TPP)Cl] < **7**. Any attempt to explain this trend must also account for the fact that neither **8** nor **9** showed a ^{59}Co resonance. Equations 7 and 8 indicate that the line width, $\omega_{1/2}$, is proportional to the square of the

(73) For example, the pK_as of benzylamine,[74] phenethylamine,[75] butylamine,[76] diethylamine,[74] and dibutylamine[74] are 9.40(8), 9.92(4), 10.66(2), 10.92, and 11.25, respectively, at 25 °C and ionic strengths of 0.0−0.1 M.

(74) Christensen, J. J.; Izatt, R. M.; Wrathall, D. P.; Hansen, L. D. *J. Chem. Soc. A* **1969**, 1212−1223.
(75) Bunting, J. W.; Stefanidis, D. *J. Am. Chem. Soc.* **1990**, *112*, 779−786.
(76) Cox, M. C.; Everett, D. H.; Landsman, D. A.; Munn, R. J. *J. Chem. Soc. B* **1968**, 1373−1379.
(77) Bernheim, R. A.; Brown, T. H.; Gutowski, H. S.; Woessner, D. E. *J. Chem. Phys.* **1959**, *30*, 950−956.
(78) Obermyer, R. T.; Jones, E. P. *J. Chem. Phys.* **1973**, *58*, 1677−1679.
(79) Fury, M.; Jones, E. P. *J. Chem. Phys.* **1976**, *65*, 2206−2210.

principal component of the EFG, q_{zz}. Clearly, a quantitative explanation of the line width variation from one Co(III) complex to the next requires determination of the EFG at the nucleus. We have used DFT methods to calculate the valence shell electron populations for all of the bis(amine) Co(III) porphyrinates of this study. The task of obtaining reliable ground state wave functions was simplified by using accurate input geometries derived from MM calculations. As shown in Table 3, the electric field gradients calculated from the Co(III) valence electron populations vary significantly depending on the type of ligand coordinated to the Co(III) ion and the conformation of the complex. More importantly, the ^{59}Co line widths increase linearly with the square of the valence EFG, q_{val} (Figure 8). This relationship holds well for the bis(amine) complexes listed in Table 3 but does not extend to the parent derivative [Co(TPP)Cl]. Thus, provided one is dealing with a class of Co(III) porphyrins with relatively similar axial ligands, it is possible to quantitatively account for the ^{59}Co line widths in terms of the magnitude of the EFG due to the valence electrons of the metal. Moreover, the good correlation of $\omega_{1/2}$ with q_{val}^2 in Figure 8 indicates that the contribution to the EFG from the ligand electrons is insignificant and may be neglected.

The fact that neither **8** nor **9** afforded a ^{59}Co NMR spectrum is indicative of a large nuclear quadrupole coupling constant (i.e., a large EFG) and a very short T_{2q}. The crucial test of the combined MM/DFT approach to delineating the electronic structures of these complexes is whether an unusually large EFG is predicted for these secondary amine derivatives. A DFT calculation (B3LYP/LACVP) on the S_4-ruffled global minimum conformation of **9** gave the following relevant Co(III) valence orbital electron populations (in units of *e*) and parameters: 4s, 0.0042; $4p_x$, 0.0015; $4p_y$, 0.0050; $4p_z$, 0.0013; $3d_{x^2-y^2}$, 0.8556; $3d_{z^2}$, 0.8883; $3d_{yz}$, 1.9623; $3d_{xz}$, 1.9672; $3d_{xy}$, 1.9750; $\langle r^{-3}\rangle_{3d}$, 4.8736; $\langle r^{-3}\rangle_{4p}$, 1.6245; q_{val}, 10.883. The value of q_{val} calculated for **9** is 2 orders of magnitude larger than that calculated for **7** (Table 3). This unusually large EFG for **9** is suggestive of a very short relaxation time, T_{2q}, and infinitely broad ^{59}Co line width, consistent with the experimental fact that no ^{59}Co resonance could be detected for this complex and the related bis(piperidine) derivative.

^{59}Co−^{14}N Coupling Constants. The $^1J_{Co-N_{ax}}$ coupling constants for **6**, **10**, and **11** measured 600(5) Hz, as evidenced by the well resolved quintet spectrum for **6** at elevated temperatures (Figure 4). More recently, we have determined a $^1J_{Co-N_{ax}}$ coupling constant of 615 Hz for [Co(TPP)(*i*-PrNH$_2$)$_2$]Cl.[80] Importantly, this is the first direct observation of ^{14}N−^{59}Co spin−spin coupling for Co(III) porphyrins. An intriguing question is why coupling to only the axially coordinated ^{14}N spins is observed for a select few of the Co(III) derivatives studied. The key requirement for the observation of ^{59}Co spin−spin coupling is that the complex has a relatively small electric field gradient and thus an intrinsically narrow ^{59}Co line width. If at a given temperature $\omega_{1/2} \leq {}^1J_{Co-N_{ax}}$, then resolution of the spin−spin coupling is possible. This is readily seen from the line width data for **6**, **10**, and **11** in Table S29. The fact that spin−spin coupling between the cobalt nucleus and the porphyrin ^{14}N nuclei is not observed strongly suggests that $^1J_{Co-N_p}$ is significantly smaller than ∼390 Hz, the narrowest line width measured in Table S29 (compound **10** at 55.1 °C). This result is consistent with Edward's estimate of 40 Hz for $^1J_{Co-N_p}$ for bis(imidazole) complexes of Co(III) *meso*-tetraarylporphyrins.[21] The porphyrin ^{14}N nuclei are therefore similar in nature to the ^{14}N nuclei of simple ammine ligands since the intrinsically small in-plane coupling constant (roughly < 100 Hz) is close in magnitude to the reported $^1J_{Co-N}$ value of 45 Hz for [Co(NH$_3$)$_6$]$^+$.[81]

MM, MD, and DFT Calculations. One of our main objectives has been to use MM, MD, and DFT calculations to help delineate the fundamental factors affecting the crystallographic conformations and ^{59}Co NMR spectra of bis(amine) complexes of Co(III) porphyrins (vide supra). An accurate force field, even if specific for metalloporphyrins, therefore underpins the theoretical work in this report. As shown in Figure 6 and Table 2, the force field parameters that we have developed provide an acceptable level of accuracy for the calculation of [Co(TPP)(amine)$_2$]$^+$ structures in the solid state. When the results of a "lattice" calculation are compared with a calculated gas phase conformation of the same molecule, the effects of crystal packing interactions on the molecular conformation are readily identified and indeed proven. The present force field has also allowed the calculation of accurate gas phase and solution phase conformations[82] of [Co(TPP)(amine)$_2$]$^+$ derivatives for which X-ray data are lacking. This has been essential for obtaining suitable input coordinates for DFT calculations (Table 3) and for predicting the low energy conformations of [Co(TPP)(1-Bu$_2$NH)$_2$]$^+$ and [Co(TPP)(Et$_2$NH)$_2$]$^+$. A challenging test of the force field parametrization is whether Marchon's highly distorted X-ray structure[2] of [Co(TMCP)((*S*)-prolinol-N)$_2$]$^+$ can be suitably matched by an MM-calculated structure. The predicted conformation is summarized by the following parameters: Co−N$_p$ = 1.951(3) Å, Co−N$_{ax}$ = 2.058(0) Å, |N$_p$| = 0.03(3) Å, |C$_a$| = 0.31(2) Å, |C$_b$| = 0.17(4) Å, and |C$_m$| = 0.65(3) Å. The data for the X-ray structure are as follows: Co−N$_p$ = 1.951(4) Å, Co−N$_{ax}$ = 2.046(1) Å, |N$_p$| = 0.02(1) Å, |C$_a$| = 0.35(2) Å, |C$_b$| = 0.24(3) Å, and |C$_m$| = 0.65(3) Å. The rmsd for a least-squares fit of the calculated structure to the X-ray structure is 0.074 Å. This level of agreement clearly indicates that the force field is capable of predicting accurate structures for bis(amine) Co(III) porphyrins that are fairly remote from those used for parametrization.

The conformational energy surface for [Co(TPP)(1-BuNH$_2$)$_2$]$^+$ shown in Figure 7 is representative of the type of surface obtained for the bis(1° amine) complexes of this study. It is also identical in symmetry to that calculated for [Fe(TPP)(1-BuNH$_2$)$_2$].[9] However, the steric energy changes are up to ∼1.5 times larger for the Co(III) derivative due to the fact that the Co−N$_{ax}$ force constant (2.65 mdyn Å^{-1}) is ∼1.4 times larger than that used for the Fe^{II}−N$_{ax}$ interaction (1.90 mdyn Å^{-1}).[9,83] Although empirically derived, these force constants do take into account the enhanced electrostatic M−L attractions in the Co(III) derivatives and thus offer a qualitatively correct picture of the energetics of axial ligand rotation for this class of compounds. Interestingly, the conformational energy surface for [Co(TPP)(Et$_2$NH)$_2$]$^+$ is significantly different to that calculated for [Co(TPP)(1-MePipz)$_2$]$^+$ (Figure S5). In addition to a lower symmetry, the changes in steric energy for [Co(TPP)(Et$_2$NH)$_2$]$^+$ are more marked; the highest energy conformations for the Et$_2$-NH derivative lie ∼2 kcal/mol above the analogous maxima for [Co(TPP)(1-MePipz)$_2$]$^+$. This mainly reflects the wider C$_\alpha$−

(80) Jamieson, S.; Munro, O. Q. Unpublished work.

(81) Jordan, R. B. *J. Magn. Reson.* **1980**, *38*, 267.

(82) The difference between a gas phase and solution phase structure is negligibly small for a solute in a nonpolar solvent and manily reflects the choice of dielectric constant for the calculation.[41]

(83) The conformational energy surface for [Co(TPP)(1-MePipz)$_2$]$^+$ (Figure S5) is very similar to that calculated previously[9] for [Fe(TPP)(Pip)$_2$]$^+$ and also shows an increase in the magnitude of the strain energy maxima by a factor of ∼1.4 relative to the surface for the Fe(II) derivative.

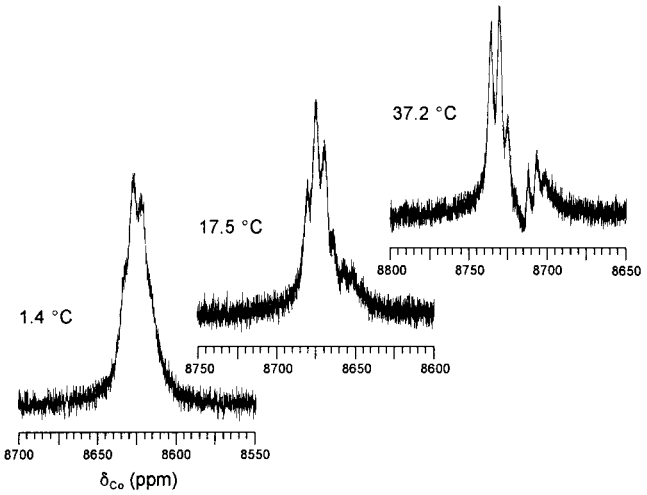

Figure 9. Selected ^{59}Co NMR spectra of [Co(TPP)(Et_2NH_2)$_2$]Cl at different temperatures in 50% (v/v) ligand/$CDCl_3$ solution. The downfield multiplet from the major conformational isomer (~78% at 37.2 °C) is assigned to the ensemble of lowest-energy S_4-ruf conformational isomers of [Co(TPP)(Et_2NH_2)$_2$]Cl; the upfield multiplet is assigned to the higher-energy planar conformations of [Co(TPP)(Et_2NH_2)$_2$]Cl.

N−C_α angles in the bis(Et_2NH) complex (111.6°), relative to those of the bis(1-MePipz) complex (107.8°), and the attendant increase in axial ligand−porphyrin core nonbonded repulsion. The latter effect is also consistent with the longer Co−N_{ax} distances for the lowest-energy gas phase conformation of [Co(TPP)(Et_2NH)$_2$]$^+$ (2.057(0) Å) relative to those calculated for [Co(TPP)(1-MePipz)$_2$]$^+$ (2.028(0) Å). The lower symmetry of the surface for [Co(TPP)(Et_2NH)$_2$]$^+$ reflects the partly staggered ethyl group configuration for the axial ligands (Figure S6); this is absent in [Co(TPP)(1-MePipz)$_2$]$^+$ since the chair conformations of the piperazine rings are rigorously maintained, favoring eclipsed N_{ax}−C_α−C_β−N torsion angles.

As noted above, the conformational energy surfaces are useful when combined with scatter plots of the MD trajectories for the [Co(TPP)(amine)$_2$]$^+$ derivatives for interpreting some of the ^{59}Co NMR data for these compounds. In particular, Figure 7 clearly shows that bis(2° amine) complexes of Co(III) porphyrins are considerably less flexible than the analogous bis(1° amine) derivatives. This difference in flexibility appears to directly affect the activation energies for molecular reorientation and hence the rotational correlation times for these complexes. One main concern is whether the calculated gas phase MM and MD data actually reflect the conformational behavior of these complexes in solution. From the calculated gas-phase population distribution for [Co(TPP)(Et_2NH)$_2$]$^+$ in Figure 7, the global minimum (S_4-ruffled porphyrin core; $\Delta U_T = 0$ kcal/mol; ϕ_1, $\phi_2 = 121°$, 344°) is largely populated at all times. However, the scatter plot also shows that the system spends part of the time in the adjacent local minimum (planar porphyrin core; ΔU_T ~3.2 kcal/mol; ϕ_1, $\phi_2 = 209°$, 344°). As shown by the ^{59}Co NMR spectra for **10** in Figure 9, two conformations with different chemical shifts do indeed coexist in solution. At 1.4 °C, the line widths of the resonances from the two conformations are broad and the separate signals cannot be distinguished. However, the line widths narrow significantly upon on warming so that the multiplets from the two conformers are sufficiently resolved at 37.2 °C. We speculate that the lower intensity signal is due to the less frequently populated local minimum with approximate C_i symmetry and a planar porphyrin core conformation (Figure S6). The total 3d electron population (7.637 e) for this conformer is marginally smaller than that for the S_4-ruffled conformation (7.644 e). From the correlation between the ^{59}Co chemical shift and $\langle r^{-3}\rangle_{3d}$ in Figure 8, one would predict similar, probably unresolvable, chemical shifts for these two species. However, the 4s electron population calculated for the planar conformer (0.259 e) is significantly larger than that calculated for the S_4-ruffled conformer (0.004 e); the higher s-electron density clearly accounts for the upfield chemical shift of the ^{59}Co resonance from the planar conformation.

Conclusions

Four new low-spin bis(amine) Co(III) porphyrins have been synthesized and structurally characterized. The X-ray data have been used in the parametrization of a molecular mechanics force field (MM+) for this class of metalloporphyrins. Together with MD and DFT calculations we have been able to show (1) that bis(1° amine) complexes are inherently more flexible than their secondary amine counterparts, (2) crystal packing interactions have a significant impact on the crystallographically observed conformations of these complexes, (3) the ^{59}Co chemical shifts depend directly on the total 3d electron population (or, more fundamentally, the radial expectation value $\langle r^{-3}\rangle_{3d}$), (4) the ^{59}Co NMR line widths are proportional to the square of the calculated electric field gradient at the cobalt nucleus, and (5) that the calculated conformational populations in the gas-phase correlate well with those observed in solution by ^{59}Co NMR spectroscopy, particularly in the case of sterically hindered bis(secondary amine) complexes. Importantly, this paper describes the unprecedented use of electronic structure theory calculations to rationalize the ^{59}Co NMR spectra of diamagnetic Co(III) porphyrins.

Acknowledgment. We thank the University of Natal (University Research Fund) and the National Research Foundation (Pretoria) for generous financial support. We would also like to express our gratitude to Leanne Cooke (University of the Witwatersrand, Johannesburg) for the low-temperature X-ray data collections and Martin C. Watson (University of Natal, Pietermaritzburg) for recording our NMR spectra and suggesting the ^{59}Co experiments.

Supporting Information Available: Crystallographic details, atomic coordinates, bond distances, bond angles, torsion angles, anisotropic thermal parameters, and hydrogen atom coordinates for compounds **1**−**4** (Tables S1−S28), ^{59}Co NMR data (Table S29), X-ray crystallographic files in CIF format, labeled ORTEP diagrams of **1** and **3**, formal diagrams of the porphyrin cores of **1** and **3**, ORTEP diagram of the H-bonding interactions in **1**, ^{1}H and ^{13}C NMR spectra for **1**, surface plots of the change in steric energy with axial ligand orientation for [Co(TPP)(1-MePipz)$_2$]$^+$, and MM-calculated conformations (S_4-ruf and planar) of [Co(TPP)(Et_2NH)$_2$]$^+$ (Figures S1−S6). This material is available free of charge via the Internet at http://pubs.acs.org.

IC000976C